



Contents lists available at ScienceDirect

## European Journal of Medicinal Chemistry

journal homepage: <http://www.elsevier.com/locate/ejmech>

## Research paper

## Targeting dual tolerant regions of binding pocket: Discovery of novel morpholine-substituted diarylpyrimidines as potent HIV-1 NNRTIs with significantly improved water solubility



Zhao Wang<sup>a</sup>, Dongwei Kang<sup>a, c, \*\*</sup>, Da Feng<sup>a</sup>, Srinivasulu Cherukupalli<sup>a</sup>, Xiangyi Jiang<sup>a</sup>, Zhipeng Fu<sup>a</sup>, Erik De Clercq<sup>b</sup>, Christophe Pannecouque<sup>b</sup>, Xinyong Liu<sup>a, c, \*\*\*</sup>, Peng Zhan<sup>a, c, \*</sup>

<sup>a</sup> Department of Medicinal Chemistry, Key Laboratory of Chemical Biology (Ministry of Education), School of Pharmaceutical Sciences, Cheeloo College of Medicine, Shandong University, 44 West Culture Road, 250012, Jinan, Shandong, PR China

<sup>b</sup> Rega Institute for Medical Research, Laboratory of Virology and Chemotherapy, K.U. Leuven, Herestraat 49 Postbus 1043 (09A097), B-3000, Leuven, Belgium

<sup>c</sup> China-Belgium Collaborative Research Center for Innovative Antiviral Drugs of Shandong Province, 44 West Culture Road, 250012, Jinan, Shandong, PR China

## ARTICLE INFO

## Article history:

Received 9 August 2020

Received in revised form

1 September 2020

Accepted 1 September 2020

Available online 10 September 2020

## Keywords:

HIV-1

NNRTIs

Tolerant region I

Tolerant region II

Morpholine

SARs

## ABSTRACT

To address the intractable issues of drug resistance and poor solubility, a novel series of morpholine-substituted diarylpyrimidines targeting the tolerant region I and tolerant region II of NNIBP were rationally designed by utilizing the available crystallography studies. The biological evaluation results showed that four most promising compounds (**14e1**, **14g1**, **14g2** and **14j2**) displayed excellent potency against WT HIV-1 strain with EC<sub>50</sub> values ranging from 58 to 87 nM, being far more potent than NVP and comparable to ETV. Besides, some derivatives exhibited moderate activity in inhibiting the mutant HIV-1 strains. More encouragingly, **14d2** (RF = 0.4) possessed higher antiresistance profile than ETV (RF = 6.3) and **K-5a2** (RF = 3.0) toward the double mutant strain F227L + V106A. The HIV-1 RT inhibition assay confirmed their binding target. The molecular docking studies were conducted and discussed in detail to rationalize the preliminary SARs. Further test indicated that morpholine could indeed promote the improvement of water solubility. Additionally, the *in silico* prediction of physicochemical properties and CYP enzymatic inhibitory ability were investigated to evaluate their drug-like features.

© 2020 Elsevier Masson SAS. All rights reserved.

\* Corresponding author. Department of Medicinal Chemistry, Key Laboratory of Chemical Biology (Ministry of Education), School of Pharmaceutical Sciences, Cheeloo College of Medicine, Shandong University, 44 West Culture Road, 250012, Jinan, Shandong, PR China.

\*\* Corresponding author. Department of Medicinal Chemistry, Key Laboratory of Chemical Biology (Ministry of Education), School of Pharmaceutical Sciences, Cheeloo College of Medicine, Shandong University, 44 West Culture Road, 250012, Jinan, Shandong, PR China.

\*\*\* Corresponding author. Department of Medicinal Chemistry, Key Laboratory of Chemical Biology (Ministry of Education), School of Pharmaceutical Sciences, Cheeloo College of Medicine, Shandong University, 44 West Culture Road, 250012, Jinan, Shandong, PR China.

E-mail addresses: [zhanpeng1982@sdu.edu.cn](mailto:zhanpeng1982@sdu.edu.cn), [zhanpeng1982@sdu.edu.cn](mailto:zhanpeng1982@sdu.edu.cn) (P. Zhan).

## 1. Introduction

Acquired immune deficiency syndrome (AIDS) is a pandemic fatal disease that seriously threatens human health worldwide, which was mainly caused by human immunodeficiency virus type 1 (HIV-1) [1]. Reverse transcriptase (RT) plays a very crucial role in the viral replication cycle, on account of its unique function of reverse transcription of single-stranded RNA into double-stranded DNA. Consequently, the HIV-1 RT has become one of the important targets for designing potent anti-HIV agents for the treatment of AIDS [2,3]. Non-nucleoside reverse transcriptase inhibitors (NNRTIs) can occupy an allosteric site (NNRTI binding pocket, NNIBP) about 10 Å distant from the RT polymerase active site, resulted in the distortion of enzyme's active site and eventually disrupting the normal functions of RT [4]. Nowadays, NNRTIs have achieved significant attraction as the most powerful and successful

component of highly active antiretroviral therapy (HAART) regimens, owing to their promising antiviral potency, modest toxicity, high specificity, and favorable pharmacokinetics profiles [5,6].

Up to now, there are six NNRTIs approved by the U.S. Food and Drug Administration (FDA) for the treatment of AIDS (Fig. 1). Nevirapine (**1**, NVP), delavirdine (**2**, DLV), and efavirenz (**3**, EFV) are first generation NNRTIs, and their clinical application was compromised by the rapid emergence of drug-resistant mutants. In particular, the K103N and Y181C are the two most prevalent single mutations selected by NVP and EFV, which displayed significantly reduced susceptibility to the first generation NNRTIs. Etravirine (**4**, ETV) and rilpivirine (**5**, RPV) approved by U.S. FDA in 2008 and 2011 respectively comprise the second generation NNRTIs, and both of them belong to the diarylpyrimidine (DAPY) family [7–9]. Besides, another new NNRTI called as doravirine (**6**, DOR) has appeared on the market in 2018 [10].

However, attributing to the low genetic barrier of resistant strains and high mutation ability of RT, new mutants with decreased susceptibility to recently approved NNRTIs have emerged, thus increasing the probability of failure of anti-HIV drug therapy. Notably, the V106A is a non-polymorphic mutation selected by NVP and DOR, which confers about 50-fold less susceptible to NVP and 5-fold less susceptible to EFV. Although V106A alone has no major impact on DOR sensitivity, it tends to cause high-level resistance to DOR in combination with other DOR-associated mutations. F227L is a non-polymorphic mutation selected by NVP and EFV that usually appears with V106A. And the combined occurrence of F227L and V106A will lead to significant reductions in NVP and EFV susceptibility [11–13]. Also, adverse effects including hepatotoxicity and hypersensitivity reactions have been observed after long-term clinical treatment. More importantly, the two DAPY-typed drugs (ETV:  $\ll 1$   $\mu\text{g/mL}$  at pH 7.0; RPV: 20  $\text{ng/mL}$  at pH 7.0) are suffering from extremely poor solubility due to their structural rigidity, leading to the undesirable pharmacokinetic properties [14,15]. In view of these current obstacles, unremitting efforts are still urgently required to develop new NNRTIs with structural diversity and improved safety profile to address the intractable issues of drug resistance and low solubility [16,17].

Our previous research work on the modifications of DAPY-typed NNRTIs has led to the identification of novel potent drug candidate **K-5a2** [18–23]. Although **K-5a2** exhibited better antiresistance profiles compared to ETV, it still has the disadvantage of poor solubility (0.05  $\mu\text{g/mL}$  at pH 7.0). Therefore, it is imperative to discover novel compounds with maintained or enhanced potency as well as improved solubility. The subsequently reported crystallographic studies of **K-5a2**/RT complexes have illustrated some important structural features, which can provide valuable insights for further structure-based optimization [24]. These features are summarized as follows: 1) the left-wing of **K-5a2** is positioned in the hydrophobic tunnel composed by highly conserved residues W229, Y188, F227, and L234 and forms hydrophobic interactions and aryl-aryl interactions with these residues; 2) the thiophene [3,2-*d*]pyrimidine central ring points to the tolerant region II and exhibits additional nonpolar interactions with the alkyl chain of E138 while maintaining hydrophobic interactions with V179 and L100; 3) the substituted benzyl-linked piperidin-4-yl-amino moieties stretches into the tolerant region I, a rather plastic groove of the binding pocket, providing extensive Van der Waals contacts and hydrogen-bonding interactions with the surrounding residues K103, V106, P225, F227, P236, and Y318; 4) the NH linker and nitrogen atom of central pyrimidine ring can develop conserved hydrogen bond or water-mediated hydrogen bond with the main chain backbone of K101.

Inspired by the binding modes between the **K-5a2** and NNIBP, we recognized that the two solvent-exposed regions, namely the tolerant region I and tolerant region II, providing an insufficiently explored chemical space for the design of novel DAPY derivatives. Besides, these two broad regions could well accommodate structurally diverse chemical moieties and involve in forming various interactions, making them potential sites worthy of more in-depth modifications. Morpholine is a privileged fragment featured in numerous approved drugs and bioactive molecules due to its superior physicochemical, biological, and easily accessible properties. There are many research examples emphasizing that morpholine not only has the potential of multiple therapeutic properties, but also can effectively modulate the drug-like parameters [25,26]. Most importantly, the non-planar structure of the alicyclic ring

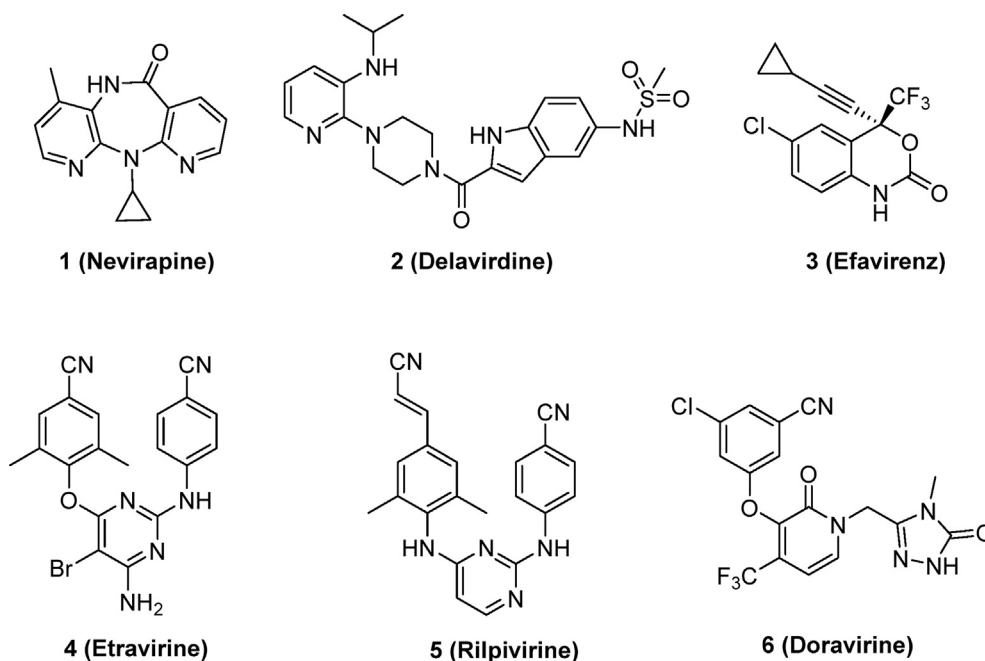


Fig. 1. Chemical structures of NNRTIs approved by the U.S. FDA.

morpholine could change the crystal packing of the original conjugated aromatic ring as well as reduce the lattice energy, thereby improving the water solubility of the molecule [27]. Recently, morpholine pharmacophore has been widely applied in drug discovery for different antiviral targets including HBV capsid assembly inhibitor GLS4 and HIV-1 NNRTIs, especially for the successful introduction of morpholine into solvent-exposed tolerant region II (7) or “NNRTI Adjacent” binding site (8) in the optimization process of NNRTIs (Fig. 2) [28–30]. More encouragingly, the previous work of our group has obtained compound 9 by introducing morpholine into the right wing of DAPYs, which exhibited significantly improved water solubility while maintaining excellent activity against the WT HIV-1 strain [31].

In the present work, we designed a series of novel DAPYs characterized by morpholine in the right-wing and different aromatic or alicyclic fused pyrimidine rings in the central scaffold via the substituent decorating and scaffold hopping strategies, for the purpose of targeting the tolerant region I and tolerant region II simultaneously (Fig. 3). Concretely, considering the cyanovinyl group of RPV may be acted as a “Michael acceptor” that covalently modifies nucleic acids, proteins, and other biological entities, so we kept the 2,6-dimethyl-4-cyanophenyl group in the left-wing unchanged to avoid potential toxicity [32]. Meanwhile, based on our previously reported studies, the privileged piperidin-4-yl-amino moiety bearing morpholine substituent was installed at the right-wing portion [31]. We expected that the introduction of hydrophilic morpholine group towards the tolerant region I may be beneficial for the improvement of solubility of new DAPYs. The function of the polar group is essentially to increase the compound hydration and to facilitate the thermodynamic process of dissolution. Simultaneously, in order to investigate the chemical space of tolerant region II, we have employed a set of fused pyrimidine rings to replace the thienopyrimidine platform, anticipating that it could effectively occupy this open area and generate additional interactions with the surrounding residues, which will contribute to the enhancement of potency against WT and resistance-associated HIV-1 strains.

Herein, we report the synthesis, biological evaluation, modeling simulation analysis of the newly designed diarylpyrimidine derivatives. Moreover, the results of preliminary structure-activity relationships (SARs), solubility measurement and other drug-like properties assessment are also be discussed comprehensively.

## 2. Results and discussion

### 2.1. Chemistry

The general synthetic routes adopted to obtain series 14a-1 are straightforwardly depicted in Scheme 1. The target compounds

14a1-2 were synthesized from the commercially available starting material 2,4-dichloropyrimidine (10a). Initially, 10a was treated with 3,5-dimethyl-4-hydroxybenzoxonitrile to obtain the intermediate 11a through nucleophilic substitution reaction. Then, 11a was reacted with 4-(*tert*-butoxycarbonyl)-aminopiperidine to generate the intermediate 12a. Next, subsequent deprotection with TFA provided the key intermediate 13a. Finally, treatment of 13a with 4-(2-chloroethyl)morpholine or 4-(2-chloroacetyl)morpholine in the presence of Cs<sub>2</sub>CO<sub>3</sub> at 60 °C yielded the final products 14a1-2. In an analogous way, other series 14b-1 were prepared [33,34]. All the newly synthesized compounds were fully characterized by means of physicochemical and spectral, and their spectral data (ESI-MS, <sup>1</sup>H NMR and <sup>13</sup>C NMR) were found to be in full agreement with the assigned molecular structures.

### 2.2. Anti-HIV activity evaluation

All the newly synthesized DAPYs derivatives were evaluated for their anti-HIV activities in MT-4 cell cultures infected with WT HIV-1 strain (IIIB) and double mutant strain K103N + Y181C (RES056) by using the MTT method. Among them, eleven compounds were selected for further evaluation of their inhibitory activities toward a panel of NNRTI resistant strains including five single mutant strains L100I, K103N, Y181C, Y188L, E138K, and double mutant strain F227L + V106A. Zidovudine (AZT), lamivudine (3TC), nevirapine (NVP), efavirenz (EFV), etravirine (ETV) were selected as the reference drugs. The biological results, expressed as EC<sub>50</sub> (anti-HIV potency), CC<sub>50</sub> (cytotoxicity) and SI (selectivity index, CC<sub>50</sub>/EC<sub>50</sub> ratio) are illustrated in Table 1 and Table 2. Additionally, the values of RF (fold-resistance factor, EC<sub>50</sub> against the mutant strain/EC<sub>50</sub> against the WT strain ratio) are summarized in Table 3.

As shown in Table 1, the biological results clearly showed that all the novel DAPYs displayed moderate to excellent potency at inhibiting WT HIV-1 strain replication with an EC<sub>50</sub> value ranging from 0.058 to 2.18 μM and SI values in the range of 52–1237, which were significantly better than that of reference drug 3TC (EC<sub>50</sub> = 5.02 μM). Among them, 20 compounds exhibited promising antiviral activity from nanomolar to sub-micromolar ranges (EC<sub>50</sub> = 0.058–0.597 μM), being more potent or equipotent compared to NVP (EC<sub>50</sub> = 0.164 μM). Especially, compounds 14e1, 14g1, 14g2 and 14j2 turned out to be the four effective inhibitors against WT HIV-1 with a double-digit nanomolar EC<sub>50</sub> value of 87 nM, 65 nM, 82 nM and 58 nM respectively, which were much superior to that of NVP and reached the considerable level of AZT (EC<sub>50</sub> = 0.019 μM). More importantly, compound 14j2 was identified as the most active derivative possessing an extremely low EC<sub>50</sub> value and high SI value, which was found to be up to 87-fold more potent than 3TC and 2.8-fold more potent than NVP, while slightly inferior to that of AZT. Moreover, most of the compounds

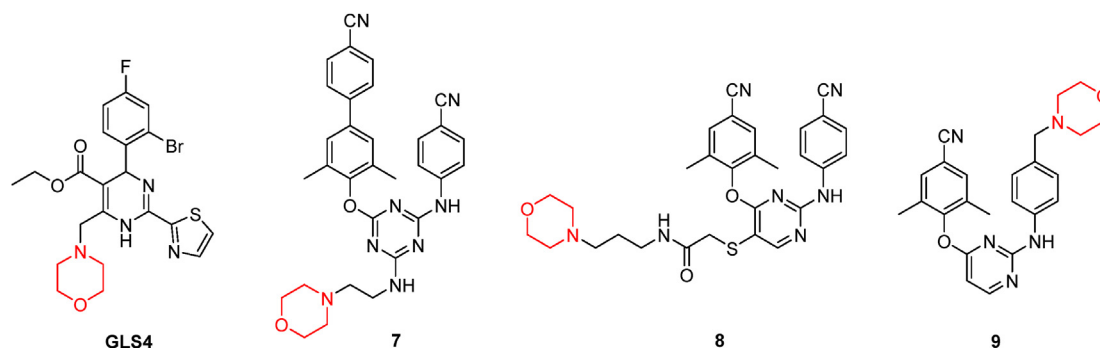


Fig. 2. Chemical structures of morpholine-containing antiviral lead compounds.

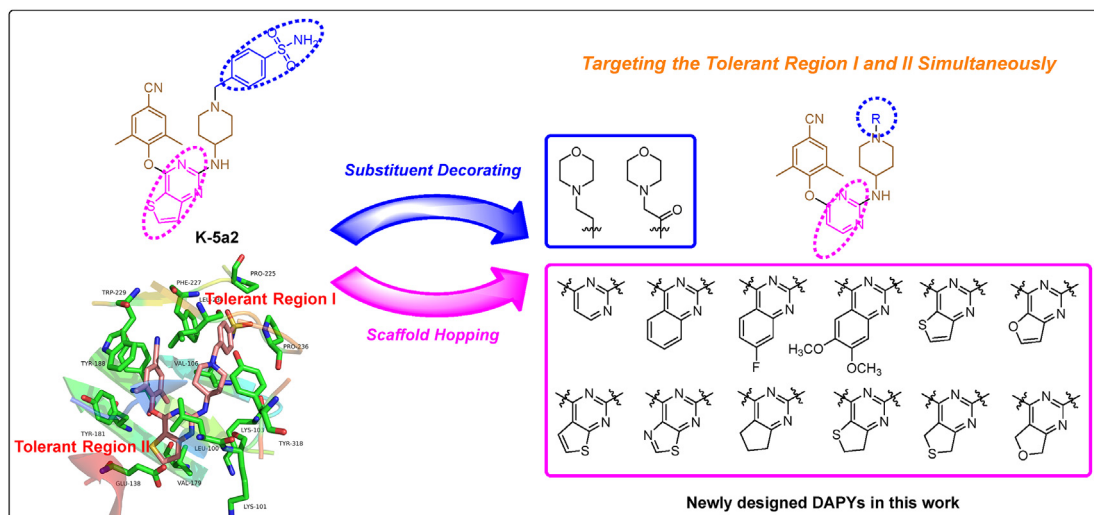
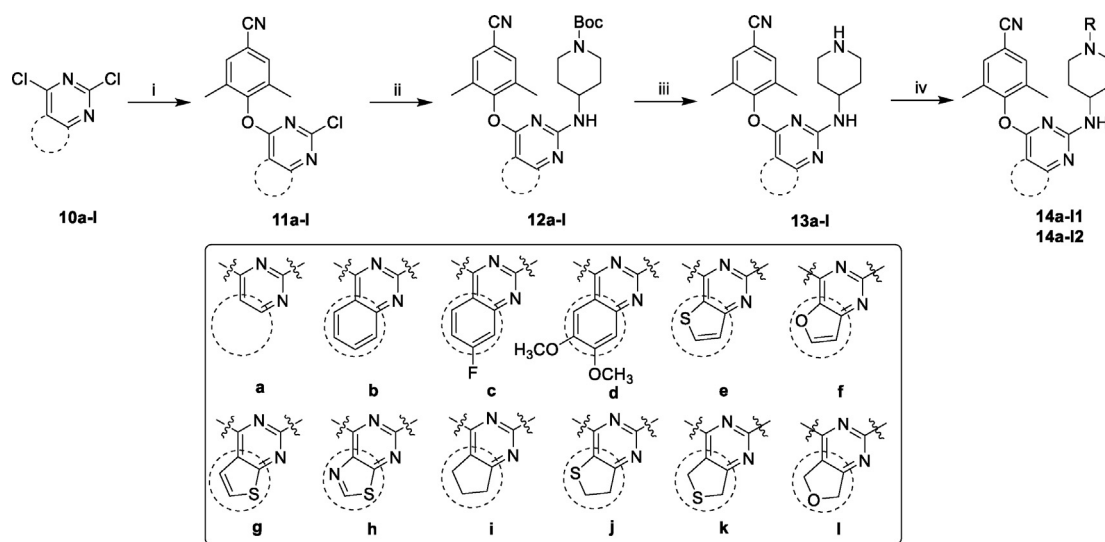


Fig. 3. Illustration of the optimization strategies for the newly designed DAPY derivatives in the present work (PDB code: 6C0J).



Scheme 1. Reagents and conditions: (i) 3,5-dimethyl-4-hydroxybenzoxonitrile, DMF,  $K_2CO_3$ , r. t.; (ii) N-(tert-butoxycarbonyl)-4-aminopiperidine, DMF,  $K_2CO_3$ , 100 °C; (iii) TFA, DCM, r. t.; (iv) 4-(2-chloroethyl)morpholine or 4-(2-chloroacetyl)morpholine, DMF,  $CS_2CO_3$ , 60 °C.

demonstrated dramatically reduced cytotoxicity compared with those reference drugs. Unfortunately, none of the target compounds showed effective inhibitory potency against the double mutant strain RES056 at the maximum tested concentration. All the compounds lost the activity toward the HIV-2 strain (ROD) as expected, which means that they are all only specific for HIV-1 and act as classical HIV-1 NNRTIs (data was not shown in the article).

Based on the anti-HIV-1 (IIIB) assay results, preliminary SARs analysis can be concluded as follows. First of all, we focused our attention on the modifications of the central scaffold and thus investigated the contribution of ring substituents varying in electronic feature and bulk to the anti-HIV activities. It is apparent that the antiviral potency is strongly dependent on the nature of the central core. With the **K-5a2** as lead, the initial part of our exploration introduced diverse aromatic-fused pyrimidine rings for the purpose of extending to the “tolerant region II” of NNIBP to enhance the resistance profiles, and 16 compounds (series **14a-h**) were designed. Just consistent with the SARs established in our previous studies, the thiophene[3,2-*d*]pyrimidine (**14e1-2**) and thiophene

[2,3-*d*]pyrimidine (**14g1-2**) proved to be more favorable for potency than other rings. It is also worth noting that the compounds **14e1-2**, which possess the same central core as the lead **K-5a2**, exhibited prominent activities among the analogues. Besides, pairwise comparison of the activities, namely **14e1** ( $EC_{50} = 0.087 \mu M$ ) and **14g1** ( $EC_{50} = 0.065 \mu M$ ), **14e2** ( $EC_{50} = 0.101 \mu M$ ) and **14g2** ( $EC_{50} = 0.082 \mu M$ ), indicated that the sulphur atom position of thiophene ring has some influence on the potency. Replacement of the central core of **14g1-2** with thiazolo[5,4-*d*]pyrimidine (**14h1**,  $EC_{50} = 0.291 \mu M$ ; **14h2**,  $EC_{50} = 0.140 \mu M$ ) resulted in slightly reduced antiviral activity against WT HIV-1, which underlined again the critical role of thiophene ring in maintaining activity. The anti-HIV activity is also strongly dependent on the type of atom incorporated in the aromatic fused ring, exemplified by compounds **14f1** ( $EC_{50} = 1.10 \mu M$ ) and **14f2** ( $EC_{50} = 0.327 \mu M$ ). And the results seems to indicate that the sulphur atom appeared to be more beneficial for the potency than the oxygen atom, probably because it can develop an extensive electrostatic interaction with Val179. Removing the fused ring yielded the pyrimidine analogues **14a1**

**Table 1**  
Antiviral activity against HIV-1 IIIB and RES056 strains and cytotoxicity of the target compounds in MT-4 cells.

Compd	Central Scaffold	R	EC <sub>50</sub> (μM) <sup>a</sup>		CC <sub>50</sub> (μM) <sup>b</sup>	SI <sup>c</sup>	
			IIIB	RES056		IIIB	RES056
<b>14a1</b>			1.12 ± 0.42	>246	246 ± 16.6	219	<1
<b>14a2</b>			0.141 ± 0.036	>143	143 ± 26.2	1016	<1
<b>14b1</b>			0.502 ± 0.23	>26.0	26.0 ± 4.47	52	<1
<b>14b2</b>			0.597 ± 0.66	>42.6	42.6 ± 15.8	71	<1
<b>14c1</b>			0.241 ± 0.061	>16.9	16.9 ± 8.48	70	<1
<b>14c2</b>			0.577 ± 0.33	>16.4	41.1 ± 14.7	71	<2.51
<b>14d1</b>			1.79 ± 0.60	>121	121 ± 6.41	68	<1
<b>14d2</b>			2.18 ± 0.67	>211	211 ± 15.4	97	<1
<b>14e1</b>			0.087 ± 0.021	>36.8	36.8 ± 10.7	423	<1
<b>14e2</b>			0.101 ± 0.045	>41.9	41.9 ± 14.6	416	<1
<b>14f1</b>			1.10 ± 0.78	>138	138 ± 8.71	125	<1
<b>14f2</b>			0.327 ± 0.13	>125	125 ± 15.9	383	<1

(continued on next page)

Table 1 (continued)

Compd	Central Scaffold	R	EC <sub>50</sub> (μM) <sup>a</sup>		CC <sub>50</sub> (μM) <sup>b</sup>	SI <sup>c</sup>	
			IIIB	RES056		IIIB	RES056
<b>14g1</b>			0.065 ± 0.021	>37.9	37.9 ± 23.7	579	<1
<b>14g2</b>			0.082 ± 0.043	>36.3	36.3 ± 11.3	442	<1
<b>14h1</b>			0.291 ± 0.089	>88.6	88.6 ± 22.0	305	<1
<b>14h2</b>			0.140 ± 0.015	>129	129 ± 5.43	919	<1
<b>14i1</b>			0.188 ± 0.065	>49.1	49.1 ± 21.0	261	<1
<b>14i2</b>			0.106 ± 0.027	>73.5	73.5 ± 14.3	696	<1
<b>14j1</b>			0.114 ± 0.029	>43.0	43.0 ± 14.4	376	<1
<b>14j2</b>			0.058 ± 0.017	>38.6	38.6 ± 11.7	663	<1
<b>14k1</b>			0.173 ± 0.096	>28.5	28.5 ± 7.59	164	<1
<b>14k2</b>			0.154 ± 0.078	>64.6	64.6 ± 37.8	420	<1
<b>14l1</b>			0.366 ± 0.12	>140	140 ± 6.38	383	<1
<b>14l2</b>			0.149 ± 0.049	>184	184 ± 3.75	1237	<1
<b>AZT</b>	—	—	0.019 ± 0.006	0.024 ± 0.007	>7.48	>397	>311
<b>3TC</b>	—	—	5.02 ± 1.93	8.35 ± 2.88	>87.2	>17	>10
<b>NVP</b>	—	—	0.164 ± 0.10	>15.0	>15.0	>92	X1 <sup>d</sup>
<b>EFV</b>	—	—	0.002 ± 0.001	0.314 ± 0.148	>6.34	>2824	>20
<b>ETV</b>	—	—	0.003 ± 0.001	0.038 ± 0.021	>4.59	>1638	>122
<b>K-5a2<sup>e</sup></b>	—	—	0.0014 ± 0.0004	0.0306 ± 0.012	>228	>159,101	>53,533

<sup>a</sup> EC<sub>50</sub>: concentration of compound required to achieve 50% protection of MT-4 cell cultures against HIV-1-induced cytotoxicity, as determined by the MTT method.

<sup>b</sup> CC<sub>50</sub>: concentration required to reduce the viability of mock-infected cell cultures by 50%, as determined by the MTT method.

<sup>c</sup> SI: selectivity index, the ratio of CC<sub>50</sub>/EC<sub>50</sub>.

<sup>d</sup> X1: ≥ 1 or < 1.

<sup>e</sup> K-5a2: the activity data were quoted from our published paper [18].

and **14a2** (EC<sub>50</sub> = 1.12 μM and 0.141 μM) with sharply decreased potency against WT HIV-1, which may be due to the disappearance of interactions with the surrounding residues of tolerant region II. What's more, compounds **14b1** and **14b2** (EC<sub>50</sub> = 0.502 μM and 0.597 μM) featuring the quinazoline central core showed acceptable potency toward HIV-1 IIIB; the introduction of fluorine atom at the C<sub>7</sub> position afforded more potent inhibitors **14c1** and **14c2** with EC<sub>50</sub> values of 0.241 and 0.577 μM, which might be attributed to the fact that the hydrogen bond donor/acceptor atom is conducive to

the improvement of activity. Conversely, the elaboration with methoxy group at the C<sub>6</sub> and C<sub>7</sub> position were detrimental to the antiviral potency; to be specific, both of **14d1** and **14d2** (EC<sub>50</sub> = 1.79 μM and 2.18 μM) showed markedly weaker activity than **14b1-2**, supposing that the 6,7-dimethoxyquinazoline ring can not fit the binding pocket well due to its larger size and rigid construction.

Meanwhile, in continuation of our exploration, considering that disrupting the planar conformation of the molecule can decrease its

**Table 2**  
Antiviral activity against several HIV-1 mutant strains of selected compounds in MT-4 cells.

Compd	EC <sub>50</sub> (μM) <sup>a</sup>					
	L100I	K103N	Y181C	Y188L	E138K	F227L + V106A
<b>14c1</b>	1.24 ± 0.24	0.522 ± 0.21	1.35 ± 0.24	2.40 ± 0.19	0.963 ± 0.18	2.92 ± 0.29
<b>14d2</b>	>211	24.8 ± 5.85	>211	>211	>211	0.974 ± 0.19
<b>14e1</b>	8.70 ± 0.90	1.04 ± 0.20	8.35 ± 1.92	9.39 ± 2.08	0.437 ± 0.10	7.14 ± 0.43
<b>14e2</b>	5.17 ± 1.18	1.38 ± 0.41	5.27 ± 0.63	4.92 ± 1.20	0.171 ± 0.05	≥17.9
<b>14g1</b>	14.7 ± 14.3	0.61 ± 0.11	6.90 ± 0.75	45.2 ± 2.89	0.586 ± 0.11	18.7 ± 21.7
<b>14g2</b>	3.67 ± 1.13	1.62 ± 0.30	3.64 ± 1.69	7.18 ± 2.83	0.334 ± 0.06	13.8 ± 2.21
<b>14h2</b>	15.1 ± 1.79	3.74 ± 1.32	3.06 ± 0.21	12.1 ± 1.46	0.703 ± 0.08	35.9 ± 5.26
<b>14i2</b>	15.9 ± 15.5	2.54 ± 0.35	10.6 ± 2.62	6.48 ± 1.38	1.12 ± 0.13	27.0 ± 7.54
<b>14j2</b>	6.12 ± 1.73	1.28 ± 0.20	5.45 ± 1.10	5.21 ± 1.48	1.31 ± 0.23	>38.6
<b>14k1</b>	16.6 ± 2.68	1.96 ± 0.45	13.2 ± 3.90	13.8 ± 0.56	1.18 ± 0.16	11.8 ± 2.08
<b>14k2</b>	24.4 ± 16.3	3.73 ± 0.99	13.4 ± 6.51	7.45 ± 0.88	0.627 ± 0.08	41.2 ± 7.10
<b>AZT</b>	0.006 ± 0.002	0.019 ± 0.005	0.016 ± 0.006	0.009 ± 0.003	0.027 ± 0.010	0.009 ± 0.003
<b>3TC</b>	1.62 ± 0.56	3.75 ± 1.13	4.79 ± 1.73	3.36 ± 0.93	6.64 ± 1.83	2.77 ± 0.75
<b>NVP</b>	1.03 ± 0.54	5.10 ± 1.00	6.69 ± 1.89	≥7.70	0.191 ± 0.064	≥5.41
<b>EFV</b>	0.040 ± 0.016	0.094 ± 0.025	0.006 ± 0.001	0.262 ± 0.080	0.005 ± 0.001	0.365 ± 0.130
<b>ETV</b>	0.005 ± 0.001	0.003 ± 0.001	0.014 ± 0.004	0.014 ± 0.005	0.007 ± 0.003	0.018 ± 0.005
<b>K-5a2<sup>b</sup></b>	0.0034 ± 0.0006	0.0029	0.0032 ± 0.0004	0.003 ± 0.0001	0.0029	0.0042 ± 0.0012

<sup>a</sup> EC<sub>50</sub>: concentration of compound required to achieve 50% protection of MT-4 cell cultures against HIV-1-induced cytotoxicity, as determined by the MTT method.

<sup>b</sup> K-5a2: the activity data were quoted from our published paper [18].

**Table 3**  
Resistance folds for several HIV-1 mutant strains of selected compounds in MT-4 cells.

Compd	Resistance folds <sup>a</sup>					
	L100I	K103N	Y181C	Y188L	E138K	F227L + V106A
<b>14c1</b>	5.1	2.2	5.6	10.0	4.0	12.1
<b>14d2</b>	>96.8	11.4	>96.8	>96.8	>96.8	0.4
<b>14e1</b>	99.9	11.9	95.8	107.9	5.0	81.9
<b>14e2</b>	51.4	13.7	52.4	48.8	1.7	≥178.1
<b>14g1</b>	224.5	9.3	105.5	690.6	9.0	285.5
<b>14g2</b>	44.8	19.8	44.3	87.5	4.1	168.0
<b>14h2</b>	107.7	26.7	21.8	86.0	5.0	256.1
<b>14i2</b>	150.4	24.1	100.8	61.4	10.6	256.0
<b>14j2</b>	105.0	21.9	93.5	89.4	22.6	>662.9
<b>14k1</b>	95.6	11.3	76.2	79.7	6.8	68.4
<b>14k2</b>	158.7	24.2	86.9	48.4	4.1	267.3
<b>AZT</b>	0.3	1.0	0.9	0.5	1.4	0.5
<b>3TC</b>	0.3	0.7	1.0	0.7	1.3	0.6
<b>NVP</b>	6.3	31.1	40.7	≥46.9	1.2	≥32.9
<b>EFV</b>	17.8	41.9	2.5	116.7	2.3	162.5
<b>ETV</b>	1.9	1.0	4.9	4.9	2.6	6.3
<b>K-5a2</b>	2.4	2.0	2.3	2.1	2.0	3.0

<sup>a</sup> Resistance fold: RF, ratio of EC<sub>50</sub> against the mutant strain/EC<sub>50</sub> against the WT strain.

lattice energy, we further introduced some alicyclic rings to the central core with the aim of improving the compounds' aqueous solubility. Among these four subseries derivatives, compounds **14j1** and **14j2** bearing 6,7-dihydrothieno[3,2-*d*]pyrimidine possessed the relatively best activity, with EC<sub>50</sub> values of 0.114 and 0.058 μM. The position of sulphur atom in the tetrahydrothiophene ring had some impact on the potency. For instance, compared with **14j1** and **14j2**, **14k1** and **14k2** (EC<sub>50</sub> = 0.173 μM and 0.154 μM) obtained by changing the position of the sulphur atom showed a slightly decreased potency. Removing the sulphur atom from the central core also led to the reduced activity, exemplified by **14i1** (EC<sub>50</sub> = 0.188 μM) and **14i2** (EC<sub>50</sub> = 0.106 μM). Analogously, incorporation of oxygen atom instead of sulphur atom impaired the anti-HIV potency (**14l1**, EC<sub>50</sub> = 0.366 μM; **14l2**, EC<sub>50</sub> = 0.149 μM), which suggested that the activity is susceptible to the kind of the atom. These observations revealed that C<sub>5</sub> position is very optimal for prominent potency and the sulphur atom is more suitable at tolerant region II. On the other hand, the effect of R groups substituted on the piperidinamine of right-wing on anti-HIV

activities was assessed and concluded that the inhibitory activity was not directly related to the type of R substituent. There was no doubt that the given conclusions are in agreement with the aforementioned SARs.

Based on the preliminary anti-HIV-1 (IIIB and RES056) activity results, we further selected some potent compounds to evaluate their ability to inhibit a variety of NNRTI-resistance mutations, including L100I, K103N, Y181C, Y188L, E138K, and F227L + V106A. **Table 2** demonstrated that all the tested compounds (except **14d2**) maintained acceptable activity against the whole mutant strains, especially against the K103N and E138K. With regard to the K103N mutant strain, which represented the most prevalent resistance-associated mutation conferring susceptibility to NVP and EFV greatly, all these compounds displayed highly potent inhibitory activities against K103N with low EC<sub>50</sub> values ranging from 0.522 to 3.74 μM, except for **14d2** (EC<sub>50</sub> = 24.8 μM). In particular, compound **14c1** provided the highest potency toward K103N, which was about 10 times and 8 times more active than NVP (EC<sub>50</sub> = 5.10 μM) and 3TC (EC<sub>50</sub> = 3.75 μM), respectively. Moreover, **14c1** (EC<sub>50(L100I)</sub> = 1.24 μM; EC<sub>50(Y181C)</sub> = 1.35 μM; EC<sub>50(Y188L)</sub> = 2.40 μM) showed the best inhibitory activities against other mutant strains L100I, Y181C, and Y188L, which were superior to or at the same magnitude as 3TC (EC<sub>50(L100I)</sub> = 1.62 μM; EC<sub>50(Y181C)</sub> = 4.79 μM; EC<sub>50(Y188L)</sub> = 3.36 μM) and NVP (EC<sub>50(L100I)</sub> = 1.03 μM; EC<sub>50(Y181C)</sub> = 6.69 μM; EC<sub>50(Y188L)</sub> ≥ 7.70 μM), suggesting that these mutants are most susceptible to **14c1**. In the case of the E138K strain, the most common mutant emerging in patients failed RPV-containing regimens, ten compounds exhibited a prominent EC<sub>50</sub> value below 1.31 μM, and more than half of them showed inhibitory activity at the submicromolar level, being far more potent than 3TC (EC<sub>50</sub> = 6.64 μM) and equivalent to NVP (EC<sub>50</sub> = 0.191 μM). As for the double mutant strain F227L + V106A, most of the compounds displayed weak or lost efficacy compared to those control drugs. Interestingly, although **14d2** was inactive towards many single mutant viruses; however, it displayed exceptionally potent activity against the F227L + V106A with an EC<sub>50</sub> value of 0.974 μM, which was much better than 3TC (EC<sub>50</sub> = 2.77 μM) and NVP (EC<sub>50</sub> ≥ 5.41 μM) and was comparable to EFV (EC<sub>50</sub> = 0.365 μM).

In addition, the resistance fold of the tested compounds were calculated in **Table 3**. To our delight, all the compounds exhibited no obvious decline in activity when it comes to K103N (RF = 2.2–26.7), because of their lower RF values compared to EFV (RF = 41.9).

Surprisingly, compound **14c1** had relatively low RF values (RF = 2.2–12.1) toward these HIV-1 mutant strains. It is speculated that the bulkier fluoroquinazoline ring of **14c1** may help to bind tightly to the RT, so that the inhibitory potency will not decrease significantly once individual amino acid mutations occurred. It was particularly noteworthy that the RF value of compound **14d2** (RF = 0.4) for F227L + V106A was less than 1, that means **14d2** possesses higher inhibitory ability against the F227L + V106A mutant strain than against the WT strain. These findings may imply that **14d2** has subtle interactions with the amino acids in the RT containing F227L and V106A. The above mentioned biological results and detailed SARs analysis verified that our original design hypothesis that introducing a morpholine group into the right-wing portion was reasonable and will be helpful to the further rational design.

### 2.3. Inhibition of HIV-1 RT

With the aim to further validate the binding target of these newly designed morpholine-substituted diarylpyrimidine derivatives, four representative compounds **14e1**, **14g1**, **14g2** and **14j2** with superior antiviral activities against WT HIV-1 strain, were selected to evaluate their ability to inhibit recombinant WT HIV-1 RT enzymes. ETV was chosen as the reference drug in this assay. As shown in Table 4, all the target compounds displayed moderate inhibitory potencies toward WT HIV-1 RT with IC<sub>50</sub> values ranging from 1.49 μM to 3.37 μM, being slightly inferior to that of ETV (IC<sub>50</sub> = 0.059 μM). Certainly, the order of enzymatic activity of these analogues was not completely consistent with the SARs of their cellular activity, which can be considered as the difference in membrane permeability, the cellular metabolism of molecules, or components of the assay system. In addition, the IC<sub>50</sub> values (micromolar level) of tested compounds including ETV are generally quite different from the EC<sub>50</sub> values (nanomolar level), probably attributing to the dependence on the test conditions or higher affinity for the full-length cellular enzyme than the recombinant RT enzyme. On the whole, the results were able to illustrate that these newly synthesized derivatives exhibited high affinity to HIV-1 RT and they all acted as typical NNRTIs.

### 2.4. Molecular modeling analysis

With the aim to better rationalize the anti-HIV potency of these newly designed compounds and to obtain further insights into their binding modes in the NNIBP of RT, the molecular docking studies of four representative compounds (**14j2**, **14c1**, **14e2** and **14d2**) were carried out by utilizing the software SurflexeDock SYBYL-X 2.0. X-ray crystal structure of HIV-1 WT RT (PDB code: 6C0J), K103N RT (PDB code: 6C0K), E138K RT (PDB code: 6C0L), RES056 RT (PDB code: 6C0R) together with F227L/V106A RT (PDB code: 6DUF) were selected as the input structures for docking calculations. The docking results were visualized by PyMOL 1.5. And the docking protocol was described in the computational section.

As shown in Fig. 4a, the binding mode of compound **14j2** with WT RT was similar to other classical DAPY-typed NNRTIs as a common horseshoe conformation in the NNIBP. Concretely, several

notable features were consistent with our previous investigations and could be described as follows: i) the left 4-cyano-2,6-dimethylphenyl moiety occupied the hydrophobic sub-pocket formed by aromatic amino acid residues Tyr181, Tyr188 and Phe 227, exhibiting extensive π–π stacking interactions with these aromatic-rich residues; ii) the central dihydrothiophene ring was oriented toward the NNIBP entrance channel, forming favorable nonpolar interactions with the alkyl chain of Glu138 and electrostatic interactions with Val179; iii) the pyrimidine N atom and NH linker developed typical double hydrogen bonds with the backbone of Lys 101 that are essential for maintaining binding affinity; iv) the right morpholine ring connected by the flexible aminopiperidine motif stretched into the protein–solvent interface and it was worth noting that the carbonyl group involves in the hydrogen bonding interactions with Lys103 and Pro236 mediated by the water molecule. Therefore, all these factors reasonably explain the excellent potency of **14j2** against the WT HIV-1 strain.

From the simulation results between K103N RT and compound **14c1**, which exhibited the most promising activity against the K103N mutant strain (Fig. 4b), it was observed that the nitrogen atom of the piperidine ring established water-mediated hydrogen bonds with the new Asn103 and Pro236 to compensate for the interactions loss caused by the Lys103 mutation. Similarly, compound **14e2** with the best anti-E138K variant activity was docked into the E138K RT (Fig. 4c). Although a certain degree of conformational distortion occurred at the terminal morpholine ring, the crucial hydrogen bonds formed by the piperidine ring with Lys103 and Pro236 through a water molecule continued to be retained.

In addition, by comparing the binding modes of **14j2** with WT RT and RES056 RT (Fig. 4d), the Y181C mutation significantly weakened the original π–π stacking interactions. On the other hand, the shift of **14j2** in the NNIBP and the conformational inversion of the carbonyl group led to the disappearance of the hydrogen bonds with Asn103 and Pro236, which provided a reasonable explanation for the sharply decreased potency against double mutant strain RES056.

Generally speaking, certain mutations of RT amino acid residues almost always result in a significant decrease in the antiviral activity of NNRTIs, especially for the double mutant strains. Intriguingly, the potency of **14d2** against the F227L + V106A strain was about 2.24-fold more potent than against WT strain. As shown in Fig. 4e and Fig. 4f, the comparative analysis of the binding modes of **14d2** with WT RT and F227L/V106A RT indicated that the much smaller side chains of Leu 227 and Ala 106 allow the chemical space of NNIBP to be further enlarged, which is more conducive to the expansion of bulky molecule to fully occupy the pocket. Furthermore, the multiple water-mediated hydrogen bonds formed by the methoxy group of the central ring with Glu138 and the nitrogen atom of piperidine ring with Lys103 and Pro236 may also contribute to the improvement of activity.

To some extent, the molecular modeling results accurately elucidated the theoretical binding modes as well as validated our original design hypothesis that introducing the privileged heterocycle morpholine into the solvent-exposed region to establish more interactions with the binding pocket, which may provide valuable clues for the follow-up structural optimization.

**Table 4**  
Inhibitory activity of compounds **14e1**, **14g1**, **14g2**, **14j2** and ETV against HIV-1 WT RT.

Compd	14e1	14g1	14g2	14j2	ETV
IC <sub>50</sub> (μM) <sup>a</sup>	2.53 ± 0.95	2.36 ± 1.15	1.49 ± 0.07	3.37 ± 1.57	0.059 ± 0.010

<sup>a</sup> IC<sub>50</sub>: inhibitory concentration of test compounds required to inhibit biotin deoxyuridine triphosphate (biotin-dUTP) incorporation into HIV-1 WT RT by 50%.

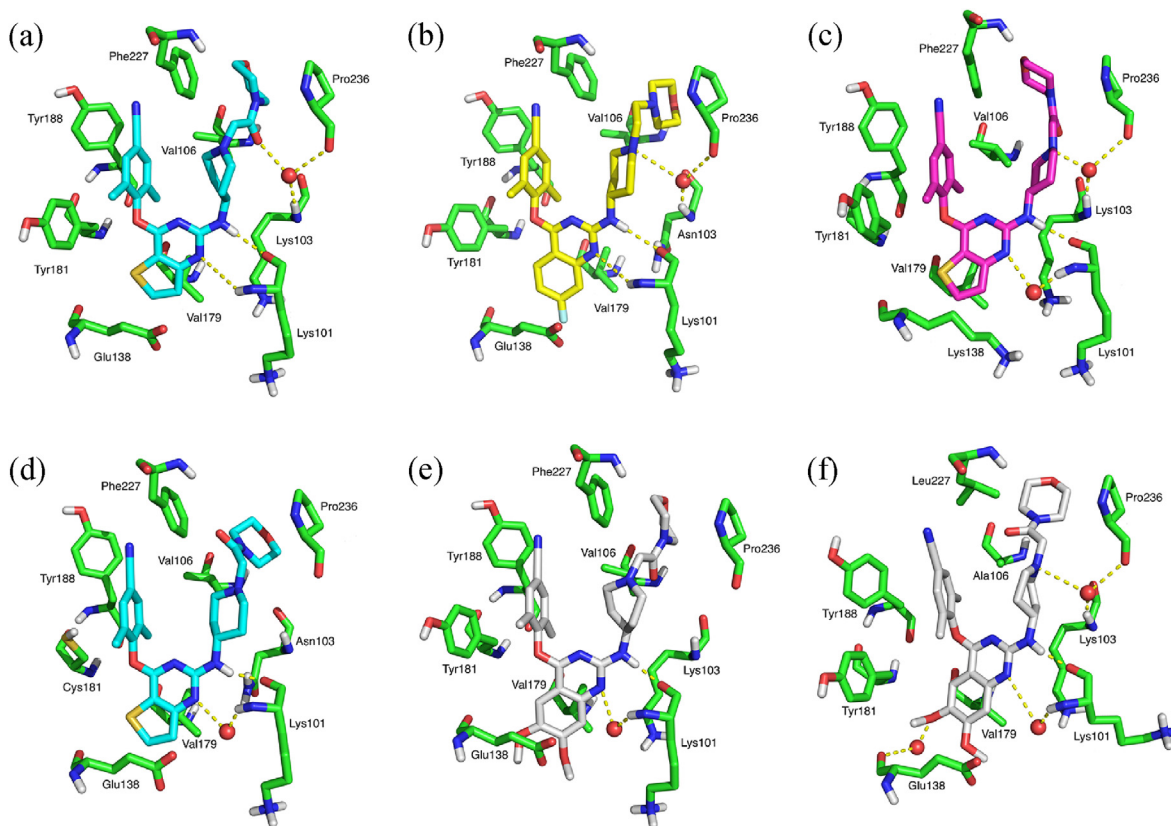


**Fig. 4.** (a) Predicted binding mode of 14j2 (cyan) with the HIV-1 WT RT (PDB code: 6CQJ). (b) Predicted binding mode of 14c1 (yellow) with the HIV-1 K103N RT (PDB code: 6COK). (c) Predicted binding mode of 14e2 (magenta) with the HIV-1 E138K RT (PDB code: 6COL). (d) Predicted binding mode of 14j2 (cyan) with the HIV-1 RES056 RT (PDB code: 6COR). (e) Predicted binding mode of 14d2 (white) with the HIV-1 WT RT (PDB code: 6CQJ). (f) Predicted binding mode of 14d2 (white) with the HIV-1 F227L/V106A RT (PDB code: 6DUF). The hydrogen bonds between the inhibitor and amino acid residues are indicated with dashed lines (yellow) and protein carbon atoms in green. The water molecules are indicated with red balls. Nonpolar hydrogen atoms are not shown for clarity.

## 2.5. Water solubility measurement

It is well known that water solubility was considered as an important physicochemical property of small molecules and occupied a major position in the early evaluation of oral drug candidates. Good water solubility often leads to accelerated absorption and thus promotes the therapeutic efficacy of the drugs. Therefore, the water solubility of compounds **14e1**, **14g1**, **14g2** and **14j2** were determined under different pH values (7.4, 7.0, and 2.0). As depicted in Table 5, all the selected compounds possessed desirable solubility at pH 2.0 (Sol. = 207–248  $\mu\text{g}/\text{mL}$ ), which were much greater than that of ETV (Sol. = 127  $\mu\text{g}/\text{mL}$ ) and equivalent to that of **K-5a2** (Sol. = 190  $\mu\text{g}/\text{mL}$ ). Compared with **K-5a2**, compound **14e1** bearing the same scaffold showed an overall improved water solubility. Among them, **14j2** displayed the optimal water solubility (Sol. = 248  $\mu\text{g}/\text{mL}$ , pH = 2.0; Sol. = 35.2  $\mu\text{g}/\text{mL}$ , pH = 7.0; Sol. = 29.1  $\mu\text{g}/\text{mL}$ , pH = 7.4). The obtained results revealed that our proposed design concept of improving the water solubility by introducing appropriate polar groups into the protein–solvent interface was completely feasible. Similarly, the morpholine as the dominant

**Table 5**  
Water solubility of compounds 14e1, 14g1, 14g2, 14j2, K-5a2 and ETV.

Compd	14e1	14g1	14g2	14j2	K-5a2 [35]	ETV [35]
pH = 7.4 ( $\mu\text{g}/\text{mL}$ )	15.6	19.7	27.6	29.1	<1	<1
pH = 7.0 ( $\mu\text{g}/\text{mL}$ )	24.4	29.3	34.2	35.2	0.05	<1
pH = 2.0 ( $\mu\text{g}/\text{mL}$ )	207	243	228	248	190	127

solubilizing group was commonly adopted in the optimization of the pharmacokinetic profiles of lead compounds, typically represented by the approved drug gefitinib.

## 2.6. In silico prediction of physicochemical properties

To further investigate the drug-like properties of representative compounds **14e1**, **14g1**, **14g2** and **14j2**, a preliminary assessment of other physicochemical properties were conducted by utilizing free online software (<http://www.molinspiration.com/>) [36]. As shown in Table 6, the results indicated that various parameters of

**Table 6**  
Physicochemical properties of compounds 14e1, 14g1, 14g2, 14j2 and ETV.

Parameter items <sup>a</sup>	Acceptable	14e1	14g1	14g2	14j2	ETV
natoms	–	35	35	36	36	28
MW	<500 Da	492.65	492.65	506.63	508.65	435.29
nON	<10	8	8	9	9	7
nOHNH	<5	1	1	1	1	3
nrotb	$\leq 10$	7	7	6	6	4
tPSA	<140 $\text{\AA}^2$	86.55	86.55	103.62	103.62	120.65
MV	–	450.93	450.93	453.11	459.30	335.95
miLog p	<5	4.58	4.58	3.90	3.47	5.03
nViol	–	0	0	1	1	1

<sup>a</sup> natoms = number of non-hydrogen atoms; MW = molecular weight; nON = number of hydrogen bond acceptors; nOHNH = number of hydrogen bond donors; nrotb = number of rotatable bonds; tPSA = topological polar surface area; MV = molar volume; miLog P = molinspiration predicted Log P; nViol = number of violations.

compounds **14e1** and **14g1** including molecular weight (MW), hydrogen bond acceptors (nON), hydrogen bond donors (nOHNH), rotatable bonds (nrotb) and  $\text{miLog } p$  were precisely consistent with the “Lipinski’s rule of five” within a definitive level. Regrettably, compounds **14g2** and **14j2** cannot meet the typical requirements due to slight deviations of their MW values. Inspiringly, all the test compounds displayed an acceptable  $\text{miLog } p$ , while the ETV go beyond the normal criteria. In terms of the topological polar surface area (tPSA), which reflects the absorption and membrane permeability of molecules, the values of all compounds were in the range of 86.55 to 103.62 Å<sup>2</sup>, confirming their advantage for intestinal absorption (<140 Å<sup>2</sup>) and impossibility to pass through the blood-brain barrier (>60 Å<sup>2</sup>), avoiding the adverse effect on the central nervous system [37].

### 2.7. In silico predicted effects of representative compounds on inhibition of CYP enzyme

According to the published clinical data, certain drugs can alter the activities or expression levels of hepatic drug metabolic enzymes, especially the cytochrome P450 (CYP), thus may causing metabolism-mediated drug–drug interactions (DDI). CYP enzymes play an essential role in the process of detoxification and bio-activation and widely involves the metabolism of more than half of the current drugs in vivo. In addition, three main subtypes CYP2C, CYP2D6 and CYP3A contribute to the majority of the CYP-mediated drug metabolism. The induction and inhibition of those CYP enzymes could lead to changes in the pharmacokinetic profile of co-administered drugs. Relevant studies have shown that ETV exhibiting inhibitory (CYP2C9, CYP2C19) and inductive (CYP3A4) properties, and it will produce DDI when co-administrating with other antiretrovirals [38]. Therefore, it is necessary to evaluate the effect of chemical molecules on the expression of CYP isozymes. In this work, we assessed the inhibitory ability of four representative compounds on the main CYP drug-metabolizing enzymes through online software (<http://admet.scbdd.com/calcpred/index/>) [39]. As described in Table 7, compounds **14e1** and **14g1** demonstrated no significant CYP enzymatic inhibition of CYP1A2, CYP2C9, CYP2C19 and CYP3A4 apart from CYP2D6. Although compound **14g2** did not inhibit CYP2D6, it displayed potential inhibitory ability against CYP2C19 as well as CYP3A4. Besides, compound **14j2** only inhibited CYP2C19 among the five CYP isozymes, while the lead compound **K-5a2** and ETV had an inhibitory effect on three different CYP enzymes.

### 3. Conclusion

In summary, to fully explore the chemical space around the tolerant region I and tolerant region II of NNIBP, a novel series of DAPY-typed HIV-1 NNRTIs bearing the morpholine moiety were rationally designed and synthesized guided by the available

**Table 7**  
Inhibitory ability on CYP1A2, CYP2C9, CYP2C19, CYP2D6 and CYP3A4 of compounds **14e1**, **14g1**, **14g2**, **14j2**, **K-5a2** and ETV.

CYP isozyme	<b>14e1</b>	<b>14g1</b>	<b>14g2</b>	<b>14j2</b>	<b>K-5a2</b>	ETV
1A2	– <sup>a</sup>	–	–	–	–	+
2C9	–	–	–	–	+	+
2C19	–	–	+	+	–	+
2D6	+ <sup>b</sup>	+	–	–	+	–
3A4	–	–	+	–	+	–

<sup>a</sup> Non-inhibitor: the probability of predicted category is less than or equal to 0.5 (minimum value is 0).

<sup>b</sup> Inhibitor: the probability of predicted category is greater than 0.5 (maximum value is 1).

structural biology information of **K-5a2**/RT complexes. Encouragingly, all the newly synthesized derivatives were found to be active against WT HIV-1 strain with EC<sub>50</sub> values in the range of 0.058–2.18 μM. Among them, four most promising compounds **14e1**, **14g1**, **14g2** and **14j2** provided double-digit nanomolar activities (EC<sub>50</sub> = 58–87 nM), being far more potent than NVP (EC<sub>50</sub> = 164 nM) and comparable to ETV (EC<sub>50</sub> = 3 nM). In terms of the HIV-1 mutant strains, compounds **14c1** (EC<sub>50(K103N)</sub> = 0.522 μM) and **14e2** (EC<sub>50(E138K)</sub> = 0.171 μM) maintained prominent activity against K103N and E138K mutant strain at the sub-micromolar scale, respectively. Furthermore, compound **14d2** exhibited moderate potency toward the F227L + V106A double mutant strain with an EC<sub>50</sub> value of 0.974 μM. It is noteworthy that the resistance fold (RF) value of **14d2** for F227L + V106A was only 0.4, which was much lower than that of ETV (RF = 6.3) and **K-5a2** (RF = 3.0). In the enzyme inhibition assay, all the selected compounds exhibited high affinity for WT HIV-1 RT and thus acted as classical NNRTIs. Molecular docking studies were performed to investigate the theoretical binding modes within the NNIBP and rationalize the preliminary SARs. Most importantly, four tested compounds **14e1**, **14g1**, **14g2** and **14j2** possessed significantly improved water solubility compared to ETV under different pH conditions. Besides, some valuable drug-like characteristics including physicochemical properties and CYP enzymatic inhibitory ability were also predicted comprehensively by using online software.

Taken together, all these results confirmed our initial design assumption that the introduction of the privileged fragment morpholine into the solvent-exposed region could achieve an optimal balance between antiviral efficacy and drug-like parameters. Currently, further optimization focused on improving the inhibitory activity toward HIV-1 mutant strains is ongoing and will be disclosed in due course.

### 4. Experimental section

#### 4.1. Chemistry

All melting points were determined on a micromelting point apparatus (Tian Jin Analytical Instrument Factory, Nankai, Tianjin, China) and were uncorrected. <sup>1</sup>H NMR and <sup>13</sup>C NMR spectra were recorded on a Bruker Avance-400 spectrometer (Bruker BioSpin, Switzerland) using DMSO-d<sub>6</sub> as the solvent and tetramethylsilane (TMS) as the internal standard. Chemical shifts are expressed as δ units (ppm) and J values are presented in hertz (Hz). Signals are abbreviated as s (singlet), d (doublet), t (triplet), q (quartet) or m (multiplet). Mass spectrometry were obtained on a LC Autosampler Device: Standard G1313A instrument. TLC was performed on Silica Gel GF254 for TLC (Merck) and spots were visualized by iodine vapors or by irradiation with UV light (λ = 254 nm). Flash column chromatography was performed on column packed with Silica Gel 60 (200–300 mesh) (Qing Dao Haiyang Chemical Company, Qingdao, China). Solvents were of reagent grade, and if necessary, were purified and dried by standard methods. Concentration of the reaction solutions involved the use of rotary evaporator at reduced pressure.

#### 4.1.1. General procedure for the synthesis of intermediates 11a-l

A reaction mixture of 4-hydroxy-3,5-dimethylbenzoxonitrile (0.15 g, 1.0 mmol) and potassium carbonate (0.17 g, 1.2 mmol) in 3 mL of DMF was stirred at room temperature for 15 min. Then the different starting material 10a-l (1.0 mmol) was added to it and stirring was continued for an additional 2 h. After completion of the reaction (monitored by TLC), the solvent was evaporated under reduced pressure, then ethyl acetate (30 mL) was added and washed with water (3 × 5 mL) and saturated brine (3 × 5 mL). The

combined organic layer was dried over anhydrous Na<sub>2</sub>SO<sub>4</sub>, filtered and concentrated, and finally recrystallized from ethyl acetate/petroleum ether (1:10) to provide the corresponding intermediates 11a-l as a white solid.

**4.1.1.1. 4-((2-chloropyrimidin-4-yl)oxy)-3,5-dimethylbenzonitrile (11a).** White solid, yield: 86.1%, mp: 126–128 °C. <sup>1</sup>H NMR (400 MHz, DMSO-d<sub>6</sub>) δ 8.70 (d, J = 5.6 Hz, 1H, C<sub>6</sub>-pyrimidine-H), 7.75 (s, 2H, C<sub>3</sub>,C<sub>5</sub>-Ph-H), 7.31 (d, J = 5.6 Hz, 1H, C<sub>5</sub>-pyrimidine-H), 2.10 (s, 6H, CH<sub>3</sub> × 2). ESI-MS: m/z 260.1 [M+H]<sup>+</sup>. C<sub>13</sub>H<sub>10</sub>ClN<sub>3</sub>O (259.05).

**4.1.1.2. 4-((2-chloroquinazolin-4-yl)oxy)-3,5-dimethylbenzonitrile (11b).** White solid, yield: 84.5%, mp: 180–182 °C. <sup>1</sup>H NMR (400 MHz, DMSO-d<sub>6</sub>) δ 8.48 (dd, J = 8.3, 1.4 Hz, 1H, C<sub>8</sub>-quinazoline-H), 8.14 (ddd, J = 8.5, 7.0, 1.5 Hz, 1H, C<sub>5</sub>-quinazoline-H), 8.00 (d, J = 8.4 Hz, 1H, C<sub>7</sub>-quinazoline-H), 7.86 (ddd, J = 8.2, 7.0, 1.1 Hz, 1H, C<sub>6</sub>-quinazoline-H), 7.78 (s, 2H, C<sub>3</sub>,C<sub>5</sub>-Ph-H), 2.14 (s, 6H, CH<sub>3</sub> × 2). ESI-MS: m/z 310.6 [M+H]<sup>+</sup>. C<sub>17</sub>H<sub>12</sub>ClN<sub>3</sub>O (309.07).

**4.1.1.3. 4-((2-chloro-7-fluoroquinazolin-4-yl)oxy)-3,5-dimethylbenzonitrile (11c).** White solid, yield: 82.9%, mp: 245–247 °C. <sup>1</sup>H NMR (400 MHz, DMSO-d<sub>6</sub>) δ 8.59 (dd, J = 8.9, 6.2 Hz, 1H, C<sub>5</sub>-fluoroquinazoline-H), 7.85 (d, J = 9.6 Hz, 1H, C<sub>8</sub>-fluoroquinazoline-H), 7.79 (s, 3H, C<sub>3</sub>,C<sub>5</sub>-Ph-H, C<sub>6</sub>-fluoroquinazoline-H), 2.14 (s, 6H, CH<sub>3</sub> × 2). ESI-MS: m/z 328.1 [M+H]<sup>+</sup>. C<sub>17</sub>H<sub>11</sub>ClF<sub>3</sub>N<sub>3</sub>O (327.06).

**4.1.1.4. 4-((2-chloro-6,7-dimethoxyquinazolin-4-yl)oxy)-3,5-dimethylbenzonitrile (11d).** White solid, yield: 79.3%, mp: 256–258 °C. <sup>1</sup>H NMR (400 MHz, DMSO-d<sub>6</sub>) δ 7.77 (s, 2H, C<sub>3</sub>,C<sub>5</sub>-Ph-H), 7.66 (s, 1H, C<sub>8</sub>-dimethoxyquinazoline-H), 7.49–7.37 (m, 1H, C<sub>5</sub>-dimethoxyquinazoline-H), 4.00 (d, J = 2.5 Hz, 6H, OCH<sub>3</sub> × 2), 2.14 (s, 6H, CH<sub>3</sub> × 2). ESI-MS: m/z 370.2 [M+H]<sup>+</sup>. C<sub>19</sub>H<sub>16</sub>ClN<sub>3</sub>O<sub>3</sub> (369.09).

**4.1.1.5. 4-((2-chlorothieno[3,2-d]pyrimidin-4-yl)oxy)-3,5-dimethylbenzonitrile (11e).** White solid, yield: 89.1%, mp: 258–260 °C. <sup>1</sup>H NMR (400 MHz, DMSO-d<sub>6</sub>) δ 8.61 (d, J = 8.6 Hz, 1H, C<sub>6</sub>-thienopyrimidine-H), 7.79 (s, 2H, C<sub>3</sub>,C<sub>5</sub>-Ph-H), 7.70 (d, J = 7.7 Hz, 1H, C<sub>7</sub>-thienopyrimidine-H), 2.14 (s, 6H, CH<sub>3</sub> × 2). ESI-MS: m/z 316.3 [M+H]<sup>+</sup>. C<sub>15</sub>H<sub>10</sub>ClN<sub>3</sub>OS (315.02).

**4.1.1.6. 4-((2-chlorofuro[3,2-d]pyrimidin-4-yl)oxy)-3,5-dimethylbenzonitrile (11f).** White solid, yield: 86.7%, mp: 225–227 °C. <sup>1</sup>H NMR (400 MHz, DMSO-d<sub>6</sub>) δ 8.66 (d, J = 2.2 Hz, 1H, C<sub>6</sub>-furopyrimidine-H), 7.78 (s, 2H, C<sub>3</sub>,C<sub>5</sub>-Ph-H), 7.32 (d, J = 2.2 Hz, 1H, C<sub>7</sub>-furopyrimidine-H), 2.14 (s, 6H, CH<sub>3</sub> × 2). ESI-MS: m/z 300.2 [M+H]<sup>+</sup>. C<sub>15</sub>H<sub>10</sub>ClN<sub>3</sub>O<sub>2</sub> (299.05).

**4.1.1.7. 4-((2-chlorothieno[2,3-d]pyrimidin-4-yl)oxy)-3,5-dimethylbenzonitrile (11g).** White solid, yield: 90.4%, mp: 269–271 °C. ESI-MS: m/z 316.3 [M+H]<sup>+</sup>. C<sub>15</sub>H<sub>10</sub>ClN<sub>3</sub>OS (315.02).

**4.1.1.8. 4-((5-chlorothiazolo[5,4-d]pyrimidin-7-yl)oxy)-3,5-dimethylbenzonitrile (11h).** White solid, yield: 85.8%, mp: 265–267 °C. <sup>1</sup>H NMR (400 MHz, DMSO-d<sub>6</sub>) δ 9.06 (s, 1H, thiazolopyrimidine-H), 7.67 (s, 2H, C<sub>3</sub>,C<sub>5</sub>-Ph-H), 2.14 (s, 6H, CH<sub>3</sub> × 2). ESI-MS: m/z 317.1 [M+H]<sup>+</sup>. C<sub>14</sub>H<sub>9</sub>ClN<sub>4</sub>OS (316.02).

**4.1.1.9. 4-((2-chloro-6,7-dihydro-5H-cyclopenta[d]pyrimidin-4-yl)oxy)-3,5-dimethylbenzonitrile (11i).** White solid, yield: 93.1%, mp: 254–256 °C. <sup>1</sup>H NMR (400 MHz, DMSO-d<sub>6</sub>) δ 7.73 (s, 2H, C<sub>3</sub>,C<sub>5</sub>-Ph-H), 3.04 (t, J = 7.8 Hz, 2H, C<sub>5</sub>-cyclopentapyrimidine-H), 2.92 (t, J = 7.7 Hz, 2H, C<sub>7</sub>-cyclopentapyrimidine-H), 2.13 (p, J = 7.7 Hz, 2H, C<sub>6</sub>-cyclopentapyrimidine-H), 2.09 (s, 6H, CH<sub>3</sub> × 2). ESI-MS: m/z 300.1 [M+H]<sup>+</sup>. C<sub>16</sub>H<sub>14</sub>ClN<sub>3</sub>O (299.08).

**4.1.1.10. 4-((2-chloro-6,7-dihydrothieno[3,2-d]pyrimidin-4-yl)oxy)-3,5-dimethylbenzonitrile (11j).** White solid, yield: 85.7%, mp: 272–274 °C. <sup>1</sup>H NMR (400 MHz, DMSO-d<sub>6</sub>) δ 7.67 (s, 2H, C<sub>3</sub>,C<sub>5</sub>-Ph-H), 3.37–3.35 (m, 2H, C<sub>7</sub>-dihydrothienopyrimidine-2H), 3.14 (t, J = 8.2 Hz, 2H, C<sub>6</sub>-dihydrothienopyrimidine-2H), 2.06 (s, 6H, CH<sub>3</sub> × 2). ESI-MS: m/z 318.2 [M+H]<sup>+</sup>. C<sub>15</sub>H<sub>12</sub>ClN<sub>3</sub>OS (317.04).

**4.1.1.11. 4-((2-chloro-5,7-dihydrothieno[3,4-d]pyrimidin-4-yl)oxy)-3,5-dimethylbenzonitrile (11k).** White solid, yield: 87.6%, mp: 268–270 °C. <sup>1</sup>H NMR (400 MHz, DMSO-d<sub>6</sub>) δ 7.72 (s, 2H, C<sub>3</sub>,C<sub>5</sub>-Ph-H), 4.12 (s, 2H, C<sub>5</sub>-dihydrothienopyrimidine-H), 4.07 (s, 2H, C<sub>7</sub>-dihydrothienopyrimidine-H), 2.10 (s, 6H, CH<sub>3</sub> × 2). ESI-MS: m/z 318.2 [M+H]<sup>+</sup>. C<sub>15</sub>H<sub>12</sub>ClN<sub>3</sub>OS (317.04).

**4.1.1.12. 4-((2-chloro-5,7-dihydrofuro[3,4-d]pyrimidin-4-yl)oxy)-3,5-dimethylbenzonitrile (11l).** White solid, yield: 82.1%, mp: 180–182 °C. <sup>1</sup>H NMR (400 MHz, DMSO-d<sub>6</sub>) δ 7.69 (s, 2H, C<sub>3</sub>,C<sub>5</sub>-Ph-H), 4.97 (s, 2H, C<sub>5</sub>-dihydrofuropyrimidine-H), 4.80 (s, 2H, C<sub>7</sub>-dihydrofuropyrimidine-H), 2.10 (s, 6H, CH<sub>3</sub> × 2). ESI-MS: m/z 302.1 [M+H]<sup>+</sup>. C<sub>15</sub>H<sub>12</sub>ClN<sub>3</sub>O<sub>2</sub> (301.06).

#### 4.1.2. General procedure for the synthesis of intermediates 13a-l

A solution of compound 11a-l (1.0 mmol), N-Boc-4-aminopiperidine (0.24 g, 1.2 mmol), and potassium carbonate (0.29 g, 2.0 mmol) in DMF was stirred overnight at 100 °C. The solution was cooled to room temperature, and ice water (30 mL) was added to it. The precipitated white solid was collected by filtration and dried to give crude 12a-l, which was used directly in the next step without further purification. Subsequently, the intermediates 12a-l (1.0 mmol) and TFA (0.75 mL, 10 mmol) were dissolved in DCM (5 mL) at room temperature, and the reaction mixture was stirred until completion monitored by TLC. Then the resulting liquid was alkalized to pH 9 with saturated sodium bicarbonate solution and the aqueous phase was extracted with DCM (3 × 10 mL). The combined organic phase was dried over anhydrous Na<sub>2</sub>SO<sub>4</sub>, filtered and concentrated. The crude residue was further purified by flash column chromatography with methanol/dichloromethane (1:10) as eluent and recrystallized from ethyl acetate/petroleum ether to give the key intermediates 13a-l as a white solid.

**4.1.2.1. 3,5-dimethyl-4-((2-(piperidin-4-ylamino)pyrimidin-4-yl)oxy)benzonitrile (13a).** White solid, yield: 74.2%, mp: 254–256 °C. <sup>1</sup>H NMR (400 MHz, DMSO-d<sub>6</sub>) δ 8.22 (d, J = 5.6 Hz, 1H, C<sub>6</sub>-pyrimidine-H), 7.68 (s, 2H, C<sub>3</sub>,C<sub>5</sub>-Ph-H), 7.24 (s, 1H, NH), 6.27 (d, J = 5.6 Hz, 1H, C<sub>5</sub>-pyrimidine-H), 3.19 (t, J = 8.1 Hz, 3H, piperidine-H), 2.97–2.59 (m, 2H, piperidine-H), 2.09 (s, 6H, CH<sub>3</sub> × 2), 1.93 (s, 1H, piperidine-NH), 1.79–1.35 (m, 4H, piperidine-H). ESI-MS: m/z 324.1 [M+H]<sup>+</sup>. C<sub>18</sub>H<sub>21</sub>N<sub>5</sub>O (323.17).

**4.1.2.2. 3,5-dimethyl-4-((2-(piperidin-4-ylamino)quinazolin-4-yl)oxy)benzonitrile (13b).** White solid, yield: 65.5%, mp: 119–121 °C. <sup>1</sup>H NMR (400 MHz, DMSO-d<sub>6</sub>) δ 8.14 (d, J = 7.8 Hz, 1H, C<sub>8</sub>-quinazoline-H), 7.75 (s, 2H, C<sub>3</sub>,C<sub>5</sub>-Ph-H), 7.48 (d, J = 8.5 Hz, 1H, C<sub>5</sub>-quinazoline-H), 7.37 (t, J = 8.6 Hz, 1H, C<sub>7</sub>-quinazoline-H), 7.30 (t, J = 7.6 Hz, 1H, C<sub>6</sub>-quinazoline-H), 4.09 (s, 1H, NH), 3.21–2.87 (m, 5H, piperidine-H), 2.13 (s, 6H, CH<sub>3</sub> × 2), 2.11 (s, 1H, piperidine-NH), 1.91–1.59 (m, 4H, piperidine-H). ESI-MS: m/z 374.5 [M+H]<sup>+</sup>. C<sub>22</sub>H<sub>23</sub>N<sub>5</sub>O (373.19).

**4.1.2.3. 4-((7-fluoro-2-(piperidin-4-ylamino)quinazolin-4-yl)oxy)-3,5-dimethylbenzonitrile (13c).** White solid, yield: 60.2%, mp: 143–145 °C. <sup>1</sup>H NMR (400 MHz, DMSO-d<sub>6</sub>) δ 8.18 (t, J = 7.5 Hz, 1H, C<sub>5</sub>-fluoroquinazoline-H), 7.73 (s, 2H, C<sub>3</sub>,C<sub>5</sub>-Ph-H), 7.26 (d, J = 7.7 Hz, 1H, NH), 7.18 (d, J = 10.8 Hz, 1H, C<sub>8</sub>-fluoroquinazoline-H), 7.12 (t, J =

8.9 Hz, 1H, C<sub>6</sub>-fluoroquinazoline-H), 4.01–3.87 (m, 1H, piperidine-H), 3.14–2.80 (m, 2H, piperidine-H), 2.66 (t, J = 12.2 Hz, 1H, piperidine-NH), 2.12 (s, 6H, CH<sub>3</sub> × 2), 2.00–1.73 (m, 2H, piperidine-H), 1.59–1.34 (m, 3H, piperidine-H), 1.31–1.14 (m, 1H, piperidine-H). ESI-MS: m/z 392.5 [M+H]<sup>+</sup>. C<sub>22</sub>H<sub>22</sub>FN<sub>5</sub>O (391.18).

4.1.2.4. 4-((6,7-dimethoxy-2-(piperidin-4-ylamino)quinazolin-4-yl)oxy)-3,5-dimethylbenzonitrile (13d). White solid, yield: 57.4%, mp: 159–161 °C. <sup>1</sup>H NMR (400 MHz, DMSO-d<sub>6</sub>) δ 7.72 (s, 2H, C<sub>3</sub>,C<sub>5</sub>-Ph-H), 7.38 (s, 1H, C<sub>8</sub>-dimethoxyquinazoline-H), 6.88 (s, 1H, C<sub>5</sub>-dimethoxyquinazoline-H), 6.68 (s, 1H, piperidine-NH), 5.33 (s, 1H, NH), 3.88 (d, J = 18.9 Hz, 6H, OCH<sub>3</sub> × 2), 3.39 (d, J = 7.6 Hz, 1H, piperidine-H), 3.06–2.72 (m, 2H, piperidine-H), 2.12 (s, 6H, CH<sub>3</sub> × 2), 1.72 (d, J = 43.0 Hz, 2H, piperidine-H), 1.24 (t, J = 7.3 Hz, 4H, piperidine-H). ESI-MS: m/z 434.3 [M+H]<sup>+</sup>. C<sub>24</sub>H<sub>27</sub>N<sub>5</sub>O<sub>3</sub> (433.21).

4.1.2.5. 3,5-dimethyl-4-((2-(piperidin-4-ylamino)thieno[3,2-d]pyrimidin-4-yl)oxy)benzonitrile (13e). White solid, yield: 84.2%, mp: 114–116 °C. <sup>1</sup>H NMR (400 MHz, DMSO-d<sub>6</sub>) δ 8.20 (d, J = 5.4 Hz, 1H, C<sub>6</sub>-thienopyrimidine-H), 7.72 (s, 2H, C<sub>3</sub>,C<sub>5</sub>-Ph-H), 7.26 (s, 1H, C<sub>7</sub>-thienopyrimidine-H), 6.92 (s, 1H, NH), 3.78 (s, 1H, piperidine-H), 2.89 (s, 2H, piperidine-H), 2.12 (s, 6H, CH<sub>3</sub> × 2), 1.74–1.78 (m, 2H, piperidine-H), 1.23–1.28 (m, 4H, piperidine-H). ESI-MS: m/z 380.5 [M+H]<sup>+</sup>. C<sub>20</sub>H<sub>21</sub>N<sub>5</sub>O<sub>2</sub> (379.15).

4.1.2.6. 3,5-dimethyl-4-((2-(piperidin-4-ylamino)furo[3,2-d]pyrimidin-4-yl)oxy)benzonitrile (13f). White solid, yield: 70.3%, mp: 123–125 °C. <sup>1</sup>H NMR (400 MHz, DMSO-d<sub>6</sub>) δ 8.23 (d, J = 2.1 Hz, 1H, C<sub>6</sub>-furopyrimidine-H), 7.78 (d, J = 8.0 Hz, 2H, C<sub>3</sub>,C<sub>5</sub>-Ph-H), 6.87 (s, 1H, C<sub>7</sub>-furopyrimidine-H), 6.77 (s, 1H, NH), 3.62 (s, 1H, piperidine-H), 2.73–2.72 (m, 2H, piperidine-H), 2.12 (s, 6H, CH<sub>3</sub> × 2), 1.72–1.53 (m, 3H, piperidine-H), 1.40–1.24 (m, 3H, piperidine-H). ESI-MS: m/z 364.1 [M+H]<sup>+</sup>. C<sub>20</sub>H<sub>21</sub>N<sub>5</sub>O<sub>2</sub> (363.17).

4.1.2.7. 3,5-dimethyl-4-((2-(piperidin-4-ylamino)thieno[2,3-d]pyrimidin-4-yl)oxy)benzonitrile (13g). White solid, yield: 66.8%, mp: 131–133 °C. <sup>1</sup>H NMR (400 MHz, DMSO-d<sub>6</sub>) δ 7.35 (d, J = 5.5 Hz, 1H, C<sub>6</sub>-thienopyrimidine-H), 7.31 (s, 2H, C<sub>3</sub>,C<sub>5</sub>-Ph-H), 7.27 (d, J = 5.9 Hz, 1H, C<sub>5</sub>-thienopyrimidine-H), 3.77 (s, 1H, NH), 3.72–3.74 (m, 1H, piperidine-H), 2.69–2.71 (m, 2H, piperidine-H), 2.10 (s, 6H, CH<sub>3</sub> × 2), 1.70–1.86 (m, 2H, piperidine-H), 1.18–1.48 (m, 4H, piperidine-H). ESI-MS: m/z 380.2 [M+H]<sup>+</sup>. C<sub>20</sub>H<sub>21</sub>N<sub>5</sub>O<sub>2</sub> (379.15).

4.1.2.8. 3,5-dimethyl-4-((5-(piperidin-4-ylamino)thiazolo[5,4-d]pyrimidin-7-yl)oxy)benzonitrile (13h). White solid, yield: 87.9%, mp: 130–132 °C. <sup>1</sup>H NMR (400 MHz, DMSO-d<sub>6</sub>) δ 9.06 (s, 1H, thiazolopyrimidine-H), 8.42 (d, J = 7.2 Hz, 1H, NH), 7.67 (s, 2H, C<sub>3</sub>,C<sub>5</sub>-Ph-H), 3.65–3.63 (m, 1H, piperidine-H), 2.79–2.78 (m, 2H, piperidine-H), 2.10 (s, 6H, CH<sub>3</sub> × 2), 1.86–1.82 (m, 2H, piperidine-H), 1.70–1.52 (m, 4H, piperidine-H). ESI-MS: m/z 381.1 [M+H]<sup>+</sup>. C<sub>19</sub>H<sub>20</sub>N<sub>6</sub>O<sub>2</sub> (380.14).

4.1.2.9. 3,5-dimethyl-4-((2-(piperidin-4-ylamino)-6,7-dihydro-5H-cyclopenta[d]pyrimidin-4-yl)oxy)benzonitrile (13i). White solid, yield: 67.2%, mp: 135–137 °C. <sup>1</sup>H NMR (400 MHz, DMSO-d<sub>6</sub>) δ 7.64 (s, 2H, C<sub>3</sub>,C<sub>5</sub>-Ph-H), 6.90 (s, 1H, NH), 3.65 (s, 1H, piperidine-H), 2.76–2.72 (m, 4H, C<sub>5</sub>,C<sub>7</sub>-cyclopentapyrimidine-H), 2.69–2.59 (m, 2H, piperidine-H), 2.07 (s, 6H, CH<sub>3</sub> × 2), 2.02–1.97 (m, 2H, C<sub>6</sub>-cyclopentapyrimidine-H), 1.81–1.21 (m, 6H, piperidine-H). ESI-MS: m/z 364.2 [M+H]<sup>+</sup>. C<sub>21</sub>H<sub>25</sub>N<sub>5</sub>O (363.21).

4.1.2.10. 3,5-dimethyl-4-((2-(piperidin-4-ylamino)-6,7-dihydrothieno[3,2-d]pyrimidin-4-yl)oxy)benzonitrile (13j). White solid, yield: 58.4%, mp: 135–137 °C. <sup>1</sup>H NMR (400 MHz,

DMSO-d<sub>6</sub>) δ 7.67 (s, 2H, C<sub>3</sub>,C<sub>5</sub>-Ph-H), 7.09 (s, 1H, NH), 3.36–3.35 (m, 3H, piperidine-H, C<sub>6</sub>-dihydrothienopyrimidine-H), 3.13 (t, J = 8.0 Hz, 2H, C<sub>7</sub>-dihydrothienopyrimidine-H), 2.71–2.62 (m, 2H, piperidine-H), 2.06 (s, 6H, CH<sub>3</sub> × 2), 1.83–1.45 (m, 6H, piperidine-H). ESI-MS: m/z 382.2 [M+H]<sup>+</sup>. C<sub>20</sub>H<sub>23</sub>N<sub>5</sub>O<sub>2</sub> (381.16).

4.1.2.11. 3,5-dimethyl-4-((2-(piperidin-4-ylamino)-5,7-dihydrothieno[3,4-d]pyrimidin-4-yl)oxy)benzonitrile (13k). White solid, yield: 63.8%, mp: 149–151 °C. <sup>1</sup>H NMR (400 MHz, DMSO-d<sub>6</sub>) δ 7.72 (s, 2H, C<sub>3</sub>,C<sub>5</sub>-Ph-H), 6.89 (s, 1H, NH), 4.12 (s, 2H, C<sub>5</sub>-dihydrothienopyrimidine-H), 4.08 (s, 2H, C<sub>7</sub>-dihydrothienopyrimidine-H), 3.72–3.70 (m, 1H, piperidine-H), 2.74–2.72 (m, 2H, piperidine-H), 2.10 (s, 6H, CH<sub>3</sub> × 2), 1.97–1.75 (m, 4H, piperidine-H), 1.47–1.42 (m, 2H, piperidine-H). ESI-MS: m/z 382.2 [M+H]<sup>+</sup>. C<sub>20</sub>H<sub>23</sub>N<sub>5</sub>O<sub>2</sub> (381.16).

4.1.2.12. 3,5-dimethyl-4-((2-(piperidin-4-ylamino)-5,7-dihydrofuro[3,4-d]pyrimidin-4-yl)oxy)benzonitrile (13l). White solid, yield: 60.7%, mp: 122–124 °C. <sup>1</sup>H NMR (400 MHz, DMSO-d<sub>6</sub>) δ 7.67 (s, 2H, C<sub>3</sub>,C<sub>5</sub>-Ph-H), 7.08 (s, 1H, NH), 4.96 (s, 2H, C<sub>5</sub>-dihydrofuropyrimidine-H), 4.77 (s, 2H, C<sub>7</sub>-dihydrofuropyrimidine-H), 3.63–3.61 (m, 1H, piperidine-H), 2.67 (s, 2H, piperidine-H), 2.09 (s, 6H, CH<sub>3</sub> × 2), 1.97–1.32 (m, 6H, piperidine-H). ESI-MS: m/z 366.2 [M+H]<sup>+</sup>. C<sub>20</sub>H<sub>23</sub>N<sub>5</sub>O<sub>2</sub> (365.19).

#### 4.1.3. General procedure for the synthesis of target compounds 14a-11 and 14a-12

The key intermediates 13a-l (1.0 mmol) were dissolved in anhydrous DMF (5 mL) in the presence of anhydrous cesium carbonate (0.39 g, 1.2 mmol), followed by the addition of corresponding 4-(2-chloroethyl)morpholine (0.17 g, 1.1 mmol) or 4-(2-chloroacetyl)morpholine (0.18 g, 1.1 mmol). The reaction solution was stirred at 60 °C and monitored by TLC until its completion. After cooling to room temperature, the solvent was removed under vacuum and water (20 mL) was added to it, followed by extraction with ethyl acetate (3 × 10 mL). The collected organic phase was washed with saturated brine (3 × 5 mL), and then dried over anhydrous Na<sub>2</sub>SO<sub>4</sub>, filtered and concentrated to obtain the crude product. Finally, the crude residue was further purified by flash column chromatography with methanol/dichloromethane (1:5) as eluent and recrystallized from ethyl acetate/petroleum ether to afford the target compounds 14a-11 and 14a-12.

4.1.3.1. 3,5-dimethyl-4-((2-((1-(2-morpholinoethyl)piperidin-4-yl)amino)pyrimidin-4-yl)oxy)benzonitrile (14a1). White solid, yield: 31.2%, mp: 138–140 °C. <sup>1</sup>H NMR (400 MHz, DMSO-d<sub>6</sub>) δ 8.20 (d, J = 5.6 Hz, 1H, C<sub>6</sub>-pyrimidine-H), 7.68 (s, 2H, C<sub>3</sub>,C<sub>5</sub>-Ph-H), 7.19 (d, J = 123.3 Hz, 1H, NH), 6.25 (d, J = 5.6 Hz, 1H, C<sub>5</sub>-pyrimidine-H), 4.09 (t, J = 5.8 Hz, 2H, morpholine-H), 3.88 (s, 2H, morpholine-H), 3.55 (t, J = 4.7 Hz, 4H, morpholine-H), 2.99 (d, J = 123.9 Hz, 2H, piperidine-H), 2.55–2.49 (m, 3H, piperidine-H), 2.42–2.37 (m, 4H, N-CH<sub>2</sub> × 2), 2.09 (s, 6H, CH<sub>3</sub> × 2), 1.68 (d, J = 74.3 Hz, 2H, piperidine-H), 1.33–1.13 (m, 2H, piperidine-H). <sup>13</sup>C NMR (100 MHz, DMSO-d<sub>6</sub>) δ 168.38, 133.10, 132.94, 119.07, 108.66, 66.32, 53.38, 52.84, 50.81, 45.71, 16.30. ESI-MS: m/z 437.20 [M+H]<sup>+</sup>. C<sub>24</sub>H<sub>32</sub>N<sub>6</sub>O<sub>2</sub> (436.26).

4.1.3.2. 3,5-dimethyl-4-((2-((1-(2-morpholino-2-oxoethyl)piperidin-4-yl)amino)pyrimidin-4-yl)oxy)benzonitrile (14a2). White solid, yield: 52.1%, mp: 187–189 °C. <sup>1</sup>H NMR (400 MHz, DMSO-d<sub>6</sub>) δ 8.19 (d, J = 5.7 Hz, 1H, C<sub>6</sub>-pyrimidine-H), 7.67 (s, 2H, C<sub>3</sub>,C<sub>5</sub>-Ph-H), 7.08 (d, J = 110.5 Hz, 1H, NH), 6.22 (d, J = 5.6 Hz, 1H, C<sub>5</sub>-pyrimidine-H), 3.53 (dt, J = 8.6, 4.4 Hz, 6H, morpholine-H), 3.42 (d, J = 4.7 Hz, 2H, morpholine-H), 3.08 (s, 2H, N-CH<sub>2</sub>), 2.95–2.59 (m, 3H, piperidine-H), 2.08 (s, 6H, CH<sub>3</sub> × 2), 1.98–1.20 (m, 6H, piperidine-H). <sup>13</sup>C NMR (100 MHz, DMSO-d<sub>6</sub>) δ 168.29, 168.18, 162.12, 160.59, 133.13, 132.93,

119.08, 108.60, 66.86, 66.71, 61.04, 52.52, 46.29, 42.13, 31.65, 16.29. ESI-MS:  $m/z$  451.18  $[M+H]^+$ .  $C_{24}H_{30}N_6O_3$  (450.24).

4.1.3.3. 3,5-dimethyl-4-((2-((1-(2-morpholinoethyl)piperidin-4-yl)amino)quinazolin-4-yl)oxy)benzotrile (14b1). White solid, yield: 44.5%, mp: 116–118 °C.  $^1H$  NMR (400 MHz, DMSO $_d$ )  $\delta$  8.13 (d,  $J$  = 8.1 Hz, 1H, C $_8$ -quinazoline-H), 7.75 (d,  $J$  = 7.1 Hz, 3H, C $_3$ , C $_5$ -Ph-H, C $_5$ -quinazoline-H), 7.47 (d,  $J$  = 8.5 Hz, 1H, C $_7$ -quinazoline-H), 7.27 (t,  $J$  = 7.5 Hz, 1H, C $_6$ -quinazoline-H), 7.08 (s, 1H, NH), 3.57 (t,  $J$  = 4.6 Hz, 6H, morpholine-H), 3.14 (s, 3H, piperidine-H), 2.48–2.26 (m, 6H, morpholine-H, N–CH $_2$   $\times$  2), 2.13 (s, 6H, CH $_3$   $\times$  2), 1.95 (d,  $J$  = 12.1 Hz, 2H, piperidine-H), 1.64 (s, 2H, piperidine-H), 1.23 (s, 2H, piperidine-H).  $^{13}C$  NMR (100 MHz, DMSO $_d$ )  $\delta$  165.32, 154.28, 135.01, 133.07, 129.23, 125.21, 123.97, 122.52, 119.05, 110.63, 108.97, 66.50, 53.79, 52.15, 29.91, 16.30. ESI-MS:  $m/z$  487.21  $[M+H]^+$ .  $C_{28}H_{34}N_6O_2$  (486.27).

4.1.3.4. 3,5-dimethyl-4-((2-((1-(2-morpholino-2-oxoethyl)piperidin-4-yl)amino)quinazolin-4-yl)oxy)benzotrile (14b2). White solid, yield: 40.8%, mp: 165–167 °C.  $^1H$  NMR (400 MHz, DMSO $_d$ )  $\delta$  8.11 (d,  $J$  = 8.1 Hz, 1H, C $_8$ -quinazoline-H), 7.74 (s, 2H, C $_3$ , C $_5$ -Ph-H), 7.68–7.62 (m, 1H, C $_5$ -quinazoline-H), 7.47 (d,  $J$  = 8.6 Hz, 1H, C $_7$ -quinazoline-H), 7.25 (t,  $J$  = 7.5 Hz, 1H, C $_6$ -quinazoline-H), 6.96 (s, 1H, NH), 3.59–3.50 (m, 6H, morpholine-H), 3.43 (q,  $J$  = 5.5, 4.6 Hz, 2H, morpholine-H), 3.14 (d,  $J$  = 5.8 Hz, 2H, N–CH $_2$ ), 2.99–2.59 (m, 3H, piperidine-H), 2.12 (d,  $J$  = 8.4 Hz, 6H, CH $_3$   $\times$  2), 2.01–1.26 (m, 6H, piperidine-H).  $^{13}C$  NMR (100 MHz, DMSO $_d$ )  $\delta$  168.17, 161.94, 154.67, 134.92, 133.58, 133.16, 133.07, 132.63, 126.60, 123.93, 123.73, 122.32, 119.05, 113.05, 108.94, 107.91, 66.86, 66.72, 61.00, 52.58, 48.70, 46.30, 42.14, 31.69, 31.25, 16.37, 16.31. ESI-MS:  $m/z$  501.14  $[M+H]^+$ .  $C_{28}H_{32}N_6O_3$  (500.25).

4.1.3.5. 4-((7-fluoro-2-((1-(2-morpholinoethyl)piperidin-4-yl)amino)quinazolin-4-yl)oxy)-3,5-dimethylbenzotrile (14c1). White solid, yield: 30.9%, mp: 169–171 °C.  $^1H$  NMR (400 MHz, DMSO $_d$ )  $\delta$  8.22 (dd,  $J$  = 8.8, 6.4 Hz, 1H, C $_5$ -fluoroquinazoline-H), 7.74 (s, 2H, C $_3$ , C $_5$ -Ph-H), 7.67 (s, 1H, NH), 7.17 (td,  $J$  = 9.5, 3.4 Hz, 2H, C $_6$ , C $_8$ -fluoroquinazoline-H), 3.60 (dt,  $J$  = 9.4, 4.5 Hz, 6H, morpholine-H), 3.06 (d,  $J$  = 7.5 Hz, 3H, piperidine-H), 2.45 (s, 6H, morpholine-H, N–CH $_2$   $\times$  2), 2.13 (s, 6H, CH $_3$   $\times$  2), 2.05–1.33 (m, 6H, piperidine-H). ESI-MS:  $m/z$  505.18  $[M+H]^+$ .  $C_{28}H_{33}FN_6O_2$  (504.26).

4.1.3.6. 4-((7-fluoro-2-((1-(2-morpholino-2-oxoethyl)piperidin-4-yl)amino)quinazolin-4-yl)oxy)-3,5-dimethylbenzotrile (14c2). White solid, yield: 34.1%, mp: 185–187 °C.  $^1H$  NMR (400 MHz, DMSO $_d$ )  $\delta$  8.18 (t,  $J$  = 7.6 Hz, 1H, C $_5$ -fluoroquinazoline-H), 7.73 (s, 2H, C $_3$ , C $_5$ -Ph-H), 7.66 (s, 1H, NH), 7.21–7.06 (m, 2H, C $_6$ , C $_8$ -fluoroquinazoline-H), 3.54 (dt,  $J$  = 9.8, 5.0 Hz, 6H, morpholine-H), 3.42 (t,  $J$  = 4.7 Hz, 2H, morpholine-H), 3.14 (s, 2H, N–CH $_2$ ), 2.96–2.58 (m, 3H, piperidine-H), 2.12 (s, 6H, CH $_3$   $\times$  2), 1.98–1.22 (m, 6H, piperidine-H).  $^{13}C$  NMR (100 MHz, DMSO $_d$ )  $\delta$  168.05 ( $J_{CF}$  = 37.9 Hz), 165.18 ( $J_{CF}$  = 39.9 Hz), 158.72, 153.60, 133.06, 133.06, 132.66, 127.09 ( $J_{CF}$  = 10.9 Hz), 119.03, 111.66 ( $J_{CF}$  = 23.1 Hz), 109.39, 109.04, 107.89 ( $J_{CF}$  = 28.1 Hz), 66.85, 66.71, 60.95, 53.93, 52.56, 48.02, 46.30, 42.12, 31.62, 16.33. ESI-MS:  $m/z$  519.21  $[M+H]^+$ .  $C_{28}H_{31}FN_6O_3$  (518.24).

4.1.3.7. 4-((6,7-dimethoxy-2-((1-(2-morpholinoethyl)piperidin-4-yl)amino)quinazolin-4-yl)oxy)-3,5-dimethylbenzotrile (14d1). White solid, yield: 40.5%, mp: 168–170 °C.  $^1H$  NMR (400 MHz, DMSO $_d$ )  $\delta$  7.72 (s, 2H, C $_3$ , C $_5$ -Ph-H), 7.39 (s, 1H, C $_8$ -dimethoxyquinazoline-H), 6.89 (s, 1H, C $_5$ -dimethoxyquinazoline-H), 6.79 (s, 1H, NH), 3.91 (s, 3H, OCH $_3$ ), 3.87 (s, 3H, OCH $_3$ ), 3.57 (t,  $J$  = 4.7 Hz, 6H, morpholine-H), 2.78 (s, 3H, piperidine-H), 2.48–2.36 (m, 6H, morpholine-H, N–CH $_2$   $\times$  2), 2.13 (s, 6H, CH $_3$   $\times$  2), 2.02–1.18 (m, 6H,

piperidine-H).  $^{13}C$  NMR (100 MHz, DMSO $_d$ )  $\delta$  164.31, 156.47, 154.13, 151.05, 146.47, 133.17, 132.93, 119.11, 108.73, 105.22, 102.32, 94.78, 66.50, 56.30, 56.21, 53.77, 52.42, 52.08, 40.44, 29.51, 16.36. ESI-MS:  $m/z$  547.22  $[M+H]^+$ .  $C_{30}H_{38}N_6O_4$  (546.30).

4.1.3.8. 4-((6,7-dimethoxy-2-((1-(2-morpholino-2-oxoethyl)piperidin-4-yl)amino)quinazolin-4-yl)oxy)-3,5-dimethylbenzotrile (14d2). White solid, yield: 43.6%, mp: 127–129 °C.  $^1H$  NMR (400 MHz, DMSO $_d$ )  $\delta$  7.71 (s, 2H, C $_3$ , C $_5$ -Ph-H), 7.38 (s, 1H, C $_8$ -dimethoxyquinazoline-H), 6.89 (s, 1H, C $_5$ -dimethoxyquinazoline-H), 6.65 (s, 1H, NH), 3.91 (s, 3H, OCH $_3$ ), 3.86 (s, 3H, OCH $_3$ ), 3.64–3.50 (m, 6H, morpholine-H), 3.44 (p,  $J$  = 4.4 Hz, 2H, morpholine-H), 3.19 (d,  $J$  = 16.2 Hz, 2H, N–CH $_2$ ), 3.01–2.67 (m, 3H, piperidine-H), 2.12 (s, 6H, CH $_3$   $\times$  2), 1.97–1.16 (m, 6H, piperidine-H).  $^{13}C$  NMR (100 MHz, DMSO $_d$ )  $\delta$  156.45, 154.89, 150.19, 147.79, 146.38, 133.19, 132.90, 108.71, 107.26, 107.01, 102.84, 66.94, 66.81, 66.67, 56.70, 56.31, 56.21, 52.67, 46.27, 42.15, 39.67, 31.87, 16.36. ESI-MS:  $m/z$  561.18  $[M+H]^+$ .  $C_{30}H_{36}N_6O_5$  (560.27).

4.1.3.9. 3,5-dimethyl-4-((2-((1-(2-morpholinoethyl)piperidin-4-yl)amino)thieno[3,2-d]pyrimidin-4-yl)oxy)benzotrile (14e1). White solid, yield: 61.7%, mp: 170–172 °C.  $^1H$  NMR (400 MHz, DMSO $_d$ )  $\delta$  8.20 (d,  $J$  = 5.5 Hz, 1H, C $_6$ -thienopyrimidine-H), 7.72 (s, 2H, C $_3$ , C $_5$ -Ph-H), 7.29 (dd,  $J$  = 26.8, 5.1 Hz, 1H, C $_7$ -thienopyrimidine-H), 6.88 (s, 1H, NH), 3.55 (t,  $J$  = 4.6 Hz, 6H, morpholine-H), 2.84 (s, 3H, piperidine-H), 2.44–2.34 (m, 6H, morpholine-H, N–CH $_2$   $\times$  2), 2.12 (s, 6H, CH $_3$   $\times$  2), 1.97–1.10 (m, 6H, piperidine-H).  $^{13}C$  NMR (100 MHz, DMSO $_d$ )  $\delta$  162.49, 160.53, 156.96, 153.45, 136.73, 133.22, 132.96, 123.99, 119.00, 109.06, 66.63, 56.29, 55.35, 54.14, 54.09, 53.03, 48.30, 31.51, 16.25. ESI-MS:  $m/z$  493.15  $[M+H]^+$ .  $C_{26}H_{32}N_6O_2S$  (492.23).

4.1.3.10. 3,5-dimethyl-4-((2-((1-(2-morpholino-2-oxoethyl)piperidin-4-yl)amino)thieno[3,2-d]pyrimidin-4-yl)oxy)benzotrile (14e2). White solid, yield: 65.2%, mp: 174–176 °C.  $^1H$  NMR (400 MHz, DMSO $_d$ )  $\delta$  8.13 (d,  $J$  = 5.5 Hz, 1H, C $_6$ -thienopyrimidine-H), 7.65 (s, 2H, C $_3$ , C $_5$ -Ph-H), 7.29–7.08 (m, 1H, C $_7$ -thienopyrimidine-H), 6.81 (s, 1H, NH), 3.47 (dd,  $J$  = 10.9, 4.9 Hz, 6H, morpholine-H), 3.36 (d,  $J$  = 4.9 Hz, 2H, morpholine-H), 3.07 (d,  $J$  = 28.7 Hz, 2H, N–CH $_2$ ), 2.75 (d,  $J$  = 50.6 Hz, 3H, piperidine-H), 2.05 (s, 6H, CH $_3$   $\times$  2), 1.86–1.14 (m, 6H, piperidine-H).  $^{13}C$  NMR (100 MHz, DMSO $_d$ )  $\delta$  168.21, 162.47, 160.55, 156.97, 153.43, 136.80, 133.23, 132.96, 124.00, 119.01, 109.05, 66.86, 66.72, 61.05, 52.57, 46.30, 42.13, 31.73, 16.26. ESI-MS:  $m/z$  507.12  $[M+H]^+$ .  $C_{26}H_{30}N_6O_3S$  (506.21).

4.1.3.11. 3,5-dimethyl-4-((2-((1-(2-morpholinoethyl)piperidin-4-yl)amino)furo[3,2-d]pyrimidin-4-yl)oxy)benzotrile (14f1). White solid, yield: 60.6%, mp: 231–233 °C.  $^1H$  NMR (400 MHz, DMSO $_d$ )  $\delta$  8.26 (d,  $J$  = 2.2 Hz, 1H, C $_6$ -furopyrimidine-H), 7.72 (s, 2H, C $_3$ , C $_5$ -Ph-H), 6.89 (s, 2H, C $_7$ -furopyrimidine-H, NH), 3.58 (t,  $J$  = 4.6 Hz, 6H, morpholine-H), 2.58 (s, 3H, piperidine-H), 2.43 (d,  $J$  = 5.2 Hz, 6H, morpholine-H, N–CH $_2$   $\times$  2), 2.13 (s, 6H, CH $_3$   $\times$  2), 2.03–1.22 (m, 6H, piperidine-H).  $^{13}C$  NMR (100 MHz, DMSO $_d$ )  $\delta$  158.86, 153.25, 152.86, 152.06, 133.22, 132.97, 127.76, 119.00, 109.05, 107.27, 66.46, 53.68, 51.79, 29.16, 16.33. ESI-MS:  $m/z$  477.28  $[M+H]^+$ .  $C_{26}H_{32}N_6O_3$  (476.25).

4.1.3.12. 3,5-dimethyl-4-((2-((1-(2-morpholino-2-oxoethyl)piperidin-4-yl)amino)furo[3,2-d]pyrimidin-4-yl)oxy)benzotrile (14f2). White solid, yield: 57.2%, mp: 177–179 °C.  $^1H$  NMR (400 MHz, DMSO $_d$ )  $\delta$  8.23 (d,  $J$  = 2.2 Hz, 1H, C $_6$ -furopyrimidine-H), 7.72 (s, 2H, C $_3$ , C $_5$ -Ph-H), 6.88 (s, 1H, C $_7$ -furopyrimidine-H), 6.74 (s, 1H, NH), 3.54 (p,  $J$  = 5.0, 4.4 Hz, 6H, morpholine-H), 3.42 (t,  $J$  = 4.7 Hz, 2H, morpholine-H), 3.09 (s, 2H, N–CH $_2$ ), 2.92–2.62 (m, 3H, piperidine-H), 2.13 (s, 6H, CH $_3$   $\times$  2), 1.93–1.21 (m, 6H, piperidine-H).  $^{13}C$  NMR

(100 MHz, DMSO<sub>d</sub><sub>6</sub>) δ 168.21, 158.97, 153.28, 152.72, 152.00, 133.23, 132.92, 127.62, 119.00, 109.01, 107.27, 66.86, 66.71, 61.09, 52.61, 46.30, 42.13, 31.75, 16.32. ESI-MS: m/z 491.21 [M+H]<sup>+</sup>. C<sub>26</sub>H<sub>30</sub>N<sub>6</sub>O<sub>4</sub> (490.23).

4.1.3.13. 3,5-dimethyl-4-((2-((1-(2-morpholinoethyl)piperidin-4-yl)amino)thieno[2,3-d]pyrimidin-4-yl)oxy)benzotrile (14g1). White solid, yield: 65.0%, mp: 153–155 °C. <sup>1</sup>H NMR (400 MHz, DMSO<sub>d</sub><sub>6</sub>) δ 7.65 (s, 2H, C<sub>3</sub>,C<sub>5</sub>-Ph-H), 7.29 (d, J = 5.9 Hz, 1H, C<sub>6</sub>-thienopyrimidine-H), 7.21 (d, J = 5.9 Hz, 1H, C<sub>5</sub>-thienopyrimidine-H), 7.05 (s, 1H, NH), 3.48 (t, J = 4.6 Hz, 6H, morpholine-H), 2.86 (s, 3H, piperidine-H), 2.38–2.26 (m, 6H, morpholine-H, N-CH<sub>2</sub> × 2), 2.04 (s, 6H, CH<sub>3</sub> × 2), 1.91–0.99 (m, 6H, piperidine-H). <sup>13</sup>C NMR (100 MHz, DMSO<sub>d</sub><sub>6</sub>) δ 162.23, 159.14, 153.67, 133.14, 132.97, 119.31, 119.05, 118.64, 108.88, 66.59, 55.90, 54.00, 52.71, 30.97, 16.33. ESI-MS: m/z 493.10 [M+H]<sup>+</sup>. C<sub>26</sub>H<sub>32</sub>N<sub>6</sub>O<sub>2</sub>S (492.23).

4.1.3.14. 3,5-dimethyl-4-((2-((1-(2-morpholino-2-oxoethyl)piperidin-4-yl)amino)thieno[2,3-d]pyrimidin-4-yl)oxy)benzotrile (14g2). White solid, yield: 61.9%, mp: 202–204 °C. <sup>1</sup>H NMR (400 MHz, DMSO<sub>d</sub><sub>6</sub>) δ 7.72 (s, 2H, C<sub>3</sub>,C<sub>5</sub>-Ph-H), 7.36 (d, J = 6.0 Hz, 1H, C<sub>6</sub>-thienopyrimidine-H), 7.27 (d, J = 6.0 Hz, 1H, C<sub>5</sub>-thienopyrimidine-H), 7.07 (s, 1H, NH), 3.54 (dt, J = 9.1, 4.8 Hz, 6H, morpholine-H), 3.42 (t, J = 4.7 Hz, 2H, morpholine-H), 3.11 (s, 2H, N-CH<sub>2</sub>), 2.94–2.60 (m, 3H, piperidine-H), 2.11 (s, 6H, CH<sub>3</sub> × 2), 2.03–1.14 (m, 6H, piperidine-H). <sup>13</sup>C NMR (100 MHz, DMSO<sub>d</sub><sub>6</sub>) δ 168.15, 162.76, 162.21, 159.14, 153.69, 133.15, 132.96, 119.24, 119.05, 118.61, 108.86, 66.85, 66.70, 60.97, 52.51, 46.28, 42.13, 36.25, 31.64, 16.32. ESI-MS: m/z 507.05 [M+H]<sup>+</sup>. C<sub>26</sub>H<sub>30</sub>N<sub>6</sub>O<sub>3</sub>S (506.21).

4.1.3.15. 3,5-dimethyl-4-((5-((1-(2-morpholinoethyl)piperidin-4-yl)amino)thiazolo[5,4-d]pyrimidin-7-yl)oxy)benzotrile (14h1). White solid, yield: 28.8%, mp: 160–162 °C. <sup>1</sup>H NMR (400 MHz, DMSO<sub>d</sub><sub>6</sub>) δ 9.01 (d, J = 43.5 Hz, 1H, thiazolopyrimidine-H), 7.70 (d, J = 22.9 Hz, 2H, C<sub>3</sub>,C<sub>5</sub>-Ph-H), 7.45 (d, J = 90.3 Hz, 1H, NH), 3.56 (q, J = 4.7 Hz, 6H, morpholine-H), 2.78 (d, J = 86.1 Hz, 3H, piperidine-H), 2.41 (d, J = 19.9 Hz, 6H, morpholine-H, N-CH<sub>2</sub> × 2), 2.11 (d, J = 8.8 Hz, 6H, CH<sub>3</sub> × 2), 1.97–1.14 (m, 6H, piperidine-H). ESI-MS: m/z 494.17 [M+H]<sup>+</sup>. C<sub>25</sub>H<sub>31</sub>N<sub>7</sub>O<sub>2</sub>S (493.23).

4.1.3.16. 3,5-dimethyl-4-((5-((1-(2-morpholino-2-oxoethyl)piperidin-4-yl)amino)thiazolo[5,4-d]pyrimidin-7-yl)oxy)benzotrile (14h2). White solid, yield: 39.2%, mp: 195–197 °C. <sup>1</sup>H NMR (400 MHz, DMSO<sub>d</sub><sub>6</sub>) δ 9.01 (d, J = 45.6 Hz, 1H, thiazolopyrimidine-H), 7.70 (d, J = 23.6 Hz, 2H, C<sub>3</sub>,C<sub>5</sub>-Ph-H), 7.62–7.23 (m, 1H, NH), 3.54 (dt, J = 8.8, 4.3 Hz, 6H, morpholine-H), 3.43 (d, J = 5.0 Hz, 2H, morpholine-H), 3.21–3.01 (m, 2H, N-CH<sub>2</sub>), 2.97–2.59 (m, 3H, piperidine-H), 2.12 (d, J = 8.3 Hz, 6H, CH<sub>3</sub> × 2), 2.06–1.09 (m, 6H, piperidine-H). <sup>13</sup>C NMR (100 MHz, DMSO<sub>d</sub><sub>6</sub>) δ 168.17, 161.17, 160.33, 156.63, 154.41, 150.20, 148.54, 133.08, 133.04, 132.76, 128.28, 119.02, 108.98, 108.26, 66.85, 66.71, 60.96, 52.55, 48.35, 46.28, 42.12, 39.67, 31.56, 31.18, 16.28. ESI-MS: m/z 508.10 [M+H]<sup>+</sup>. C<sub>25</sub>H<sub>29</sub>N<sub>7</sub>O<sub>3</sub>S (507.21).

4.1.3.17. 3,5-dimethyl-4-((2-((1-(2-morpholinoethyl)piperidin-4-yl)amino)-6,7-dihydro-5H-cyclopenta[d]pyrimidin-4-yl)oxy)benzotrile (14i1). White solid, yield: 50.4%, mp: 184–186 °C. <sup>1</sup>H NMR (400 MHz, DMSO<sub>d</sub><sub>6</sub>) δ 7.65 (s, 2H, C<sub>3</sub>,C<sub>5</sub>-Ph-H), 6.81 (d, J = 77.9 Hz, 1H, NH), 3.55 (t, J = 4.6 Hz, 6H, morpholine-H), 2.77 (dt, J = 21.8, 7.5 Hz, 7H, C<sub>5</sub>,C<sub>7</sub>-cyclopentapyrimidine-H, piperidine-H), 2.44–2.31 (m, 6H, morpholine-H, N-CH<sub>2</sub> × 2), 2.08 (s, 6H, CH<sub>3</sub> × 2), 2.03 (d, J = 7.7 Hz, 2H, C<sub>6</sub>-cyclopentapyrimidine-H), 1.89–1.13 (m, 6H, piperidine-H). <sup>13</sup>C NMR (100 MHz, DMSO<sub>d</sub><sub>6</sub>) δ 164.33, 162.04, 154.30, 133.16, 132.63, 119.16, 108.32, 66.59, 55.87, 53.99, 52.69, 39.66, 34.22, 31.17, 25.95, 22.04, 16.32. ESI-MS: m/z

477.22 [M+H]<sup>+</sup>. C<sub>27</sub>H<sub>36</sub>N<sub>6</sub>O<sub>2</sub> (476.29).

4.1.3.18. 3,5-dimethyl-4-((2-((1-(2-morpholino-2-oxoethyl)piperidin-4-yl)amino)-6,7-dihydro-5H-cyclopenta[d]pyrimidin-4-yl)oxy)benzotrile (14i2). White solid, yield: 56.1%, mp: 212–214 °C. <sup>1</sup>H NMR (400 MHz, DMSO<sub>d</sub><sub>6</sub>) δ 7.65 (s, 2H, C<sub>3</sub>,C<sub>5</sub>-Ph-H), 6.76 (d, J = 92.5 Hz, 1H, NH), 3.53 (dq, J = 8.5, 4.4 Hz, 6H, morpholine-H), 3.41 (t, J = 4.7 Hz, 2H, morpholine-H), 3.06 (s, 2H, N-CH<sub>2</sub>), 2.76 (dt, J = 20.5, 7.5 Hz, 7H, C<sub>5</sub>,C<sub>7</sub>-cyclopentapyrimidine-H, piperidine-H), 2.08 (s, 6H, CH<sub>3</sub> × 2), 2.03 (d, J = 7.9 Hz, 2H, C<sub>6</sub>-cyclopentapyrimidine-H), 1.94–1.08 (m, 6H, piperidine-H). <sup>13</sup>C NMR (100 MHz, DMSO<sub>d</sub><sub>6</sub>) δ 168.18, 164.31, 162.07, 154.29, 133.15, 132.59, 119.16, 108.30, 66.86, 66.70, 61.08, 52.50, 46.29, 42.12, 34.21, 31.72, 25.96, 22.05, 16.32. ESI-MS: m/z 491.21 [M+H]<sup>+</sup>. C<sub>27</sub>H<sub>34</sub>N<sub>6</sub>O<sub>3</sub> (490.27).

4.1.3.19. 3,5-dimethyl-4-((2-((1-(2-morpholinoethyl)piperidin-4-yl)amino)-6,7-dihydrothieno[3,2-d]pyrimidin-4-yl)oxy)benzotrile (14j1). White solid, yield: 45.7%, mp: 188–190 °C. <sup>1</sup>H NMR (400 MHz, DMSO<sub>d</sub><sub>6</sub>) δ 7.67 (s, 2H, C<sub>3</sub>,C<sub>5</sub>-Ph-H), 7.03 (s, 1H, NH), 3.56 (s, 6H, morpholine-H), 3.36 (t, J = 8.2 Hz, 2H, C<sub>6</sub>-dihydrothienopyrimidine-H), 3.15 (t, J = 8.1 Hz, 2H, C<sub>7</sub>-dihydrothienopyrimidine-H), 2.93 (s, 3H, piperidine-H), 2.42 (d, J = 32.4 Hz, 6H, morpholine-H, N-CH<sub>2</sub> × 2), 2.07 (s, 6H, CH<sub>3</sub> × 2), 1.82–0.92 (m, 6H, piperidine-H). <sup>13</sup>C NMR (100 MHz, DMSO<sub>d</sub><sub>6</sub>) δ 162.01, 160.57, 153.94, 133.08, 132.74, 119.06, 108.66, 66.55, 53.89, 52.34, 36.95, 30.60, 29.33, 16.25. ESI-MS: m/z 495.21 [M+H]<sup>+</sup>. C<sub>26</sub>H<sub>34</sub>N<sub>6</sub>O<sub>2</sub>S (494.25).

4.1.3.20. 3,5-dimethyl-4-((2-((1-(2-morpholino-2-oxoethyl)piperidin-4-yl)amino)-6,7-dihydrothieno[3,2-d]pyrimidin-4-yl)oxy)benzotrile (14j2). White solid, yield: 50.8%, mp: 201–203 °C. <sup>1</sup>H NMR (400 MHz, DMSO<sub>d</sub><sub>6</sub>) δ 7.67 (s, 2H, C<sub>3</sub>,C<sub>5</sub>-Ph-H), 6.93 (d, J = 80.6 Hz, 1H, NH), 3.53 (q, J = 5.3 Hz, 6H, morpholine-H), 3.41 (t, J = 4.7 Hz, 2H, morpholine-H), 3.37 (d, J = 8.2 Hz, 2H, N-CH<sub>2</sub>), 3.13 (dd, J = 22.3, 14.2 Hz, 4H, C<sub>6</sub>,C<sub>7</sub>-dihydrothienopyrimidine-H), 2.94–2.59 (m, 3H, piperidine-H), 2.07 (s, 6H, CH<sub>3</sub> × 2), 1.97–1.09 (m, 6H, piperidine-H). <sup>13</sup>C NMR (100 MHz, DMSO<sub>d</sub><sub>6</sub>) δ 168.09, 162.00, 160.61, 153.89, 133.08, 132.68, 119.07, 108.64, 66.84, 66.69, 60.96, 52.42, 46.26, 42.12, 36.92, 31.57, 29.33, 16.25. ESI-MS: m/z 509.20 [M+H]<sup>+</sup>. C<sub>26</sub>H<sub>32</sub>N<sub>6</sub>O<sub>3</sub>S (508.23).

4.1.3.21. 3,5-dimethyl-4-((2-((1-(2-morpholinoethyl)piperidin-4-yl)amino)-5,7-dihydrothieno[3,4-d]pyrimidin-4-yl)oxy)benzotrile (14k1). White solid, yield: 52.1%, mp: 119–121 °C. <sup>1</sup>H NMR (400 MHz, DMSO<sub>d</sub><sub>6</sub>) δ 7.67 (s, 2H, C<sub>3</sub>,C<sub>5</sub>-Ph-H), 7.15 (d, J = 97.8 Hz, 1H, NH), 4.11 (d, J = 23.1 Hz, 4H, C<sub>5</sub>,C<sub>7</sub>-dihydrothienopyrimidine-H), 3.56 (t, J = 4.6 Hz, 6H, morpholine-H), 2.95 (d, J = 56.1 Hz, 3H, piperidine-H), 2.47–2.26 (m, 6H, morpholine-H, N-CH<sub>2</sub> × 2), 2.09 (s, 6H, CH<sub>3</sub> × 2), 1.96–0.90 (m, 6H, piperidine-H). <sup>13</sup>C NMR (100 MHz, DMSO<sub>d</sub><sub>6</sub>) δ 164.47, 162.14, 133.07, 132.79, 119.06, 108.67, 66.53, 53.87, 52.32, 30.95, 30.52, 16.28. ESI-MS: m/z 495.22 [M+H]<sup>+</sup>. C<sub>26</sub>H<sub>34</sub>N<sub>6</sub>O<sub>2</sub>S (494.25).

4.1.3.22. 3,5-dimethyl-4-((2-((1-(2-morpholino-2-oxoethyl)piperidin-4-yl)amino)-5,7-dihydrothieno[3,4-d]pyrimidin-4-yl)oxy)benzotrile (14k2). White solid, yield: 57.4%, mp: 167–169 °C. <sup>1</sup>H NMR (400 MHz, DMSO<sub>d</sub><sub>6</sub>) δ 7.67 (s, 2H, C<sub>3</sub>,C<sub>5</sub>-Ph-H), 7.33–6.84 (m, 1H, NH), 4.27–3.88 (m, 4H, C<sub>5</sub>,C<sub>7</sub>-dihydrothienopyrimidine-H), 3.57–3.48 (m, 6H, morpholine-H), 3.41 (t, J = 4.7 Hz, 2H, morpholine-H), 3.09 (d, J = 19.3 Hz, 2H, N-CH<sub>2</sub>), 2.95–2.61 (m, 3H, piperidine-H), 2.09 (d, J = 3.4 Hz, 6H, CH<sub>3</sub> × 2), 1.88–0.93 (m, 6H, piperidine-H). <sup>13</sup>C NMR (100 MHz, DMSO<sub>d</sub><sub>6</sub>) δ 168.04, 164.46, 162.18, 133.08, 132.79, 119.07, 108.66, 66.84, 66.69, 60.86, 52.42, 46.26, 42.12, 31.48, 30.99, 16.28. ESI-MS: m/z 509.19 [M+H]<sup>+</sup>. C<sub>26</sub>H<sub>32</sub>N<sub>6</sub>O<sub>3</sub>S (508.23).

4.1.3.23. 3,5-dimethyl-4-((2-((1-(2-morpholinoethyl)piperidin-4-yl)amino)-5,7-dihydrofuro[3,4-d]pyrimidin-4-yl)oxy)benzotrile (1411). White solid, yield: 50.8%, mp: 173–175 °C. <sup>1</sup>H NMR (400 MHz, DMSO-d<sub>6</sub>) δ 7.67 (s, 2H, C<sub>3</sub>,C<sub>5</sub>-Ph-H), 7.20 (d, J = 82.9 Hz, 1H, NH), 4.97 (d, J = 2.3 Hz, 2H, C<sub>5</sub>-dihydrofuro-pyrimidine-H), 4.78 (s, 2H, C<sub>7</sub>-dihydrofuro-pyrimidine-H), 3.55 (t, J = 4.6 Hz, 6H, morpholine-H), 2.87 (d, J = 41.8 Hz, 3H, piperidine-H), 2.46–2.30 (m, 6H, morpholine-H, N-CH<sub>2</sub> × 2), 2.10 (s, 6H, CH<sub>3</sub> × 2), 1.98–1.11 (m, 6H, piperidine-H). <sup>13</sup>C NMR (100 MHz, DMSO-d<sub>6</sub>) δ 162.95, 162.49, 133.14, 132.94, 119.05, 108.75, 69.39, 66.59, 55.86, 54.96, 54.01, 52.72, 39.64, 31.07, 16.27. ESI-MS: m/z 479.22 [M+H]<sup>+</sup>. C<sub>26</sub>H<sub>34</sub>N<sub>6</sub>O<sub>3</sub> (478.27).

4.1.3.24. 3,5-dimethyl-4-((2-((1-(2-morpholino-2-oxoethyl)piperidin-4-yl)amino)-5,7-dihydrofuro[3,4-d]pyrimidin-4-yl)oxy)benzotrile (1412). White solid, yield: 61.2%, mp: 184–186 °C. <sup>1</sup>H NMR (400 MHz, DMSO-d<sub>6</sub>) δ 7.67 (s, 2H, C<sub>3</sub>,C<sub>5</sub>-Ph-H), 7.16 (d, J = 87.7 Hz, 1H, NH), 4.96 (s, 2H, C<sub>5</sub>-dihydrofuro-pyrimidine-H), 4.77 (s, 2H, C<sub>7</sub>-dihydrofuro-pyrimidine-H), 3.60–3.48 (m, 6H, morpholine-H), 3.41 (t, J = 4.7 Hz, 2H, morpholine-H), 3.08 (s, 2H, N-CH<sub>2</sub>), 2.98–2.60 (m, 3H, piperidine-H), 2.10 (s, 6H, CH<sub>3</sub> × 2), 1.99–1.03 (m, 6H, piperidine-H). <sup>13</sup>C NMR (100 MHz, DMSO-d<sub>6</sub>) δ 168.15, 162.99, 162.49, 133.14, 132.88, 119.04, 108.74, 69.41, 66.85, 66.70, 61.00, 52.44, 46.28, 42.12, 31.59, 16.27. ESI-MS: m/z 493.15 [M+H]<sup>+</sup>. C<sub>26</sub>H<sub>32</sub>N<sub>6</sub>O<sub>4</sub> (492.25).

#### 4.2. In vitro anti-HIV assay

Evaluation of the anti-HIV activity and cytotoxicity of the target compounds was performed by utilizing the MTT method in MT-4 cells described previously [40,41]. Stock solutions (10 × final concentration) of test compounds were added in 25 μL volumes to two series of triplicate wells to allow simultaneous evaluation of their effects on mock- and HIV-infected cells at the beginning of each experiment. Serial five-fold dilutions of test compounds were prepared directly in flat-bottomed 96-well microtiter trays by adding 100 μL medium to the 25 μL stock solution and transferring 25 μL of this solution to another well that contained 100 μL medium using a Biomek 3000 robot (Beckman Instruments, Fullerton, CA). Each sample includes untreated control HIV- and mock-infected cell samples. HIV-1 WT strain (IIIB), HIV-1 drug-resistant strains including K103N + Y181C (RES056), L100I, K103N, Y181C, Y188L, E138K and F227L + V106A or HIV-2 strain (ROD) stock (50 μL) at 100–300 CCID<sub>50</sub> (50% cell culture infectious dose) or culture medium was added to either the infected or mock-infected wells of the microtiter tray. Mock-infected cells were used to evaluate the effect of test compounds on uninfected cells in order to evaluate its cytotoxicity. Exponentially growing MT-4 cells were centrifuged for 5 min at 1000 rpm and the supernatant was discarded. The MT-4 cells were resuspended at 6 × 10<sup>5</sup> cells/mL, and then transferred 50 μL volumes to the microtiter tray wells. After infection five days, the viability of mock- and HIV-infected cells was examined spectrophotometrically by the MTT assay. The 50% cytotoxic concentration (CC<sub>50</sub>) was defined as the concentration of the test compound that reduced the viability of the mock-infected MT-4 cells by 50%. The 50% effective concentration (EC<sub>50</sub>) was defined as the concentration of the test compound achieving 50% protection from the cytopathic effect of the virus in infected cells.

#### 4.3. HIV-1 RT inhibition assay

A HIV-1 reverse transcriptase (RT) assay kit produced by Roche was used for the RT inhibition assay [42]. All the reagents for performing the RT reaction came from the kit and the ELSIA procedures for RT inhibition assay were conducted following the

description in the kit protocol. In brief, the reaction mixture containing template/primer complex, viral nucleotides (dNTPs) and HIV-1 reverse transcriptase (RT) enzyme in the incubation buffer with or without inhibitors was incubated for 1 h at 37 °C. Subsequently, the reaction mixture was transferred to a streptavidin coated microtiter plate (MTP) and incubated for another 1 h at 37 °C to ensure the retranscriptional cDNA chain that consisted biotin labeled dNTPs bound to streptavidin. Then used washing buffer to remove the unbound dNTPs and anti-DIG-POD working solution was added. After incubation for 1 h at 37 °C, the DIG-labeled dNTPs incorporated in cDNA were bound to the anti-DIG-POD antibody. The unbound anti-DIG-PODs were removed and the peroxidesubstrate (ABST) solution was added to the MTPs. A colored reaction proceeds during cleavage of the substrate catalyzed by POD. The absorbance of the sample was determined at O.D. 405 nm using a microtiter plate ELISA reader. The percentage inhibitory activity of RT inhibitors was calculated by formula as given below:

$$\% \text{ Inhibition} = \frac{[\text{O.D. value with RT but without inhibitors} - \text{O.D. value with RT and inhibitors}]}{[\text{O.D. value with RT and inhibitors} - \text{O.D. value without RT and inhibitors}]}$$

The IC<sub>50</sub> values corresponded to the concentrations of the test compounds required to inhibit the incorporation of biotin-dUTP into RT by 50%.

#### 4.4. Molecular simulation

Molecular modeling was performed with the Tripos molecular modeling packages Sybyl-X 2.0. All the molecules (**14j2**, **14c1**, **14e2** and **14d2**) for docking were built using standard bond lengths and angles from Sybyl-X 2.0/Base Builder and were optimized using the Tripos force field for 1000-generations two times or more until the maximum derivative of energy became 0.005 kcal/(mol\*Å). Charges were computed and added according to Gasteiger–Huckel parameters. The published five dimensional crystal structures of RT complexes {HIV-1 WT RT (PDB code: 6COJ), K103N RT (PDB code: 6COK), E138K RT (PDB code: 6COL), RES056 RT (PDB code: 6COR) and F227L/V106A RT (PDB code: 6DUF)} were retrieved from the Protein Data Bank and were used for the docking experiment by means of the surflex-docking module of Sybyl-X 2.0. The protein was prepared by removing the ligand, water molecules, and other unnecessary small molecules from the crystal structure of the ligand HIV-1 RT complex before docking; polar hydrogen atoms and charges were added to the protein. After the protomol was generated, which referred to a computational representation of the intended binding site to which putative ligands are aligned, the optimized compounds **14j2**, **14c1**, **14e2** or **14d2** was surflex-docked into the NNIBP, with the relevant parameters set as defaults. The original ligand of the coordinates was used as a reference molecule to calculate the RMSD values. The docking scores related to binding affinities were calculated based on hydrophobic, polar, and repulsive interactions as well as entropic effects and solvation. Top-scoring pose was shown by the software of PyMOL version 1.5 (<http://www.pymol.org/>). The secondary structure of RT was shown in cartoons, and only the key residues for interactions with the inhibitor were labeled and shown in sticks. The potential hydrogen bonds were presented by dashed lines.

#### 4.5. Water solubility measurement

Water solubility was measured in phosphate buffer at three different pH conditions. The compound was initially weighed in three orders of magnitude, namely approximately 0.01 mg, 0.1 mg and 1 mg, and then it was dissolved in the phosphate buffer of the same pH value until the solution was clear [43]. The average value of water solubility was calculated from the weight of the compound

and the volume of the solution. The assays were measured at least in duplicate.

### Declaration of competing interest

The authors declare that they have no known competing financial interests or personal relationships that could have appeared to influence the work reported in this paper.

### Acknowledgments

We gratefully acknowledge the financial support from the National Natural Science Foundation of China (NSFC Nos. 81973181 and 81903453), the Key Project of NSFC for International Cooperation (No. 81420108027), Shandong Provincial Natural Science Foundation (ZR2019BH011), China Postdoctoral Science Foundation (2019T120596), Shandong Provincial Key Research and Development Project (Nos. 2017CXGC1401 and 2019JZZY021011), and the Taishan Scholar Program at Shandong Province. We thank K. Erven, K. Uyttersprot and C. Heens for technical assistance with the anti-HIV assays.

### Appendix A. Supplementary data

Supplementary data to this article can be found online at <https://doi.org/10.1016/j.ejmech.2020.112811>.

### References

- [1] R.J. Shattock, M. Warren, S. McCormack, C.A. Hankins, AIDS. Turning the tide against HIV, *Science* 333 (2011) 42–43.
- [2] P. Zhan, C. Pannecouque, E. De Clercq, X. Liu, Anti-HIV drug discovery and development: current innovations and future trends, *J. Med. Chem.* 59 (2016) 2849–2878.
- [3] N. Sluis-Cremer, Future of nonnucleoside reverse transcriptase inhibitors, *Proc. Natl. Acad. Sci. U.S.A.* 115 (2018) 637–638.
- [4] G. Bec, B. Meyer, M.A. Gerard, J. Steger, K. Fauster, P. Wolff, D. Burnouf, R. Micura, P. Dumas, E. Ennifar, Thermodynamics of HIV-1 reverse transcriptase in action elucidates the mechanism of action of non-nucleoside inhibitors, *J. Am. Chem. Soc.* 135 (2013) 9743–9752.
- [5] V. Namasivayam, M. Vanangamudi, V.G. Kramer, S. Kurup, P. Zhan, X. Liu, J. Kongsted, S.N. Byrereddy, The journey of HIV-1 non-nucleoside reverse transcriptase inhibitors (NNRTIs) from lab to clinic, *J. Med. Chem.* 62 (2019) 4851–4883.
- [6] J. Du, J. Guo, D. Kang, Z. Li, G. Wang, J. Wu, Z. Zhang, H. Fang, X. Hou, Z. Huang, G. Li, X. Lu, X. Liu, L. Ouyang, L. Rao, P. Zhan, X. Zhang, Y. Zhang, New techniques and strategies in drug discovery, *Chin. Chem. Lett.* 31 (2020) 1695–1708.
- [7] C. Flexner, HIV drug development: the next 25 years, *Nat. Rev. Drug Discov.* 6 (2007) 959–966.
- [8] S.X. Gu, H.H. Lu, G.Y. Liu, X.L. Ju, Y.Y. Zhu, Advances in diarylpyrimidines and related analogues as HIV-1 nonnucleoside reverse transcriptase inhibitors, *Eur. J. Med. Chem.* 158 (2018) 371–392.
- [9] L. Battini, M. Bollini, Challenges and approaches in the discovery of human immunodeficiency virus type-1 non-nucleoside reverse transcriptase inhibitors, *Med. Res. Rev.* 39 (2019) 1235–1273.
- [10] E.D. Deeks, Doravirine: first global approval, *Drugs* 78 (2018) 1643–1650.
- [11] M. Feng, D. Wang, J.A. Grobler, D.J. Hazuda, M.D. Miller, M.T. Lai, In vitro resistance selection with doravirine (MK-1439), a novel nonnucleoside reverse transcriptase inhibitor with distinct mutation development pathways, *Antimicrob. Agents Chemother.* 59 (2015) 590–598.
- [12] G. Sterrantino, V. Borghi, A.P. Callegaro, B. Bruzzone, F. Saladini, F. Maggiolo, G. Maffongelli, M. Andreoni, M. De Gennaro, N. Gianotti, P. Bagnarelli, A. Vergori, A. Antinori, M. Zazzi, M. Zaccarelli, ARCA Study Group, Prevalence of predicted resistance to doravirine in HIV-1-positive patients after exposure to non-nucleoside reverse transcriptase inhibitors, *Int. J. Antimicrob. Agents* 53 (2019) 515–519.
- [13] C. Soulie, M.M. Santoro, C. Charpentier, A. Storto, D. Paraskevis, D. Di Carlo, W. Gennari, G. Sterrantino, M. Zazzi, C.F. Perno, V. Calvez, D. Descamps, F. Ceccherini-Silberstein, A.G. Marcelin, Rare occurrence of doravirine resistance-associated mutations in HIV-1-infected treatment-naïve patients, *J. Antimicrob. Chemother.* 74 (2019) 614–617.
- [14] P. Zhan, X. Chen, D. Li, Z. Fang, E. De Clercq, X. Liu, HIV-1 NNRTIs: structural diversity, pharmacophore similarity, and implications for drug design, *Med. Res. Rev.* 33 (2013) E1–E72.
- [15] C. Beyrer, A. Pozniak, HIV drug resistance - an emerging threat to epidemic control, *N. Engl. J. Med.* 377 (2017) 1605–1607.
- [16] Y. Wu, C. Tang, R. Rui, L. Yang, W. Ding, J. Wang, Y. Li, C.C. Lai, Y. Wang, R. Luo, W. Xiao, H. Zhang, Y. Zheng, Y. He, Synthesis and biological evaluation of a series of 2-((5-alkyl/aryl-1H-pyrazol-3-yl)methyl)thio)-5-alkyl-6-(cyclohexylmethyl)-pyrimidin-4(3H)-ones as potential HIV-1 inhibitors, *Acta Pharm. Sin. B* 10 (2020) 512–518.
- [17] E. De Clercq, An Odyssey in antiviral drug development-50 years at the Rega Institute: 1964-2014, *Acta Pharm. Sin. B* 5 (2015) 520–543.
- [18] D. Kang, Z. Fang, Z. Li, B. Huang, H. Zhang, X. Lu, H. Xu, Z. Zhou, X. Ding, D. Daelemans, E. De Clercq, C. Pannecouque, P. Zhan, X. Liu, Design, synthesis, and evaluation of thiophene[3,2-d]pyrimidine derivatives as HIV-1 non-nucleoside reverse transcriptase inhibitors with significantly improved drug resistance profiles, *J. Med. Chem.* 59 (2016) 7991–8007.
- [19] D. Kang, Z. Fang, B. Huang, X. Lu, H. Zhang, H. Xu, Z. Huo, Z. Zhou, Z. Yu, Q. Meng, G. Wu, X. Ding, Y. Tian, D. Daelemans, E. De Clercq, C. Pannecouque, P. Zhan, X. Liu, Structure-based optimization of thiophene[3,2-d]pyrimidine derivatives as potent HIV-1 non-nucleoside reverse transcriptase inhibitors with improved potency against resistance-associated variants, *J. Med. Chem.* 60 (2017) 4424–4443.
- [20] D. Kang, T. Zhao, Z. Wang, D. Feng, H. Zhang, B. Huang, G. Wu, F. Wei, Z. Zhou, L. Jing, X. Zuo, Y. Tian, V. Poongavanam, J. Kongsted, E. De Clercq, C. Pannecouque, P. Zhan, X. Liu, Discovery of piperidine-substituted thiazolo [5,4-d]pyrimidine derivatives as potent and orally bioavailable HIV-1 non-nucleoside reverse transcriptase inhibitors, *Commun. Chem.* 2 (2019) 74.
- [21] D. Kang, D. Feng, T. Ginex, J. Zou, F. Wei, T. Zhao, B. Huang, Y. Sun, S. Desta, E. De Clercq, C. Pannecouque, P. Zhan, X. Liu, Exploring the hydrophobic channel of NNIBP leads to the discovery of novel piperidine-substituted thiophene[3,2-d]pyrimidine derivatives as potent HIV-1 NNRTIs, *Acta Pharm. Sin. B* 10 (2020) 878–894.
- [22] D. Kang, F.X. Ruiz, D. Feng, A. Pilch, T. Zhao, F. Wei, Z. Wang, Y. Sun, Z. Fang, E. De Clercq, C. Pannecouque, E. Arnold, X. Liu, P. Zhan, Discovery and characterization of fluorine-substituted diarylpyrimidine derivatives as novel HIV-1 NNRTIs with highly improved resistance profiles and low activity for the hERG ion channel, *J. Med. Chem.* 63 (2020) 1298–1312.
- [23] D. Kang, D. Feng, Y. Sun, Z. Fang, F. Wei, E. De Clercq, C. Pannecouque, X. Liu, P. Zhan, Structure-based bioisosterism yields HIV-1 NNRTIs with improved drug-resistance profiles and favorable pharmacokinetic properties, *J. Med. Chem.* 63 (2020) 4837–4848.
- [24] Y. Yang, D. Kang, L.A. Nguyen, Z.B. Smithline, C. Pannecouque, P. Zhan, X. Liu, T.A. Steitz, Structural basis for potent and broad inhibition of HIV-1 RT by thiophene[3,2-d]pyrimidine non-nucleoside inhibitors, *eLife* 7 (2018), e36340.
- [25] A.P. Kourounakis, D. Xanthopoulos, A. Tzara, Morpholine as a privileged structure: a review on the medicinal chemistry and pharmacological activity of morpholine containing bioactive molecules, *Med. Res. Rev.* 40 (2020) 709–752.
- [26] X. Jiang, J. Yu, Z. Zhou, J. Kongsted, Y. Song, C. Pannecouque, E. De Clercq, D. Kang, V. Poongavanam, X. Liu, P. Zhan, Molecular design opportunities presented by solvent-exposed regions of target proteins, *Med. Res. Rev.* 39 (2019) 2194–2238.
- [27] W. Wei, S. Cherukupalli, L. Jing, X. Liu, P. Zhan, Fsp<sup>3</sup>: a new parameter for drug-likeness, *Drug Discov. Today* (2020), <https://doi.org/10.1016/j.drudis.2020.07.017>.
- [28] Q. Ren, X. Liu, Z. Luo, J. Li, C. Wang, S. Goldmann, J. Zhang, Y. Zhang, Discovery of hepatitis B virus capsid assembly inhibitors leading to a heteroaryl-dihydropyrimidine based clinical candidate (GLS4), *Bioorg. Med. Chem.* 25 (2017) 1042–1056.
- [29] K. Jin, M. Liu, C. Zhuang, E. De Clercq, C. Pannecouque, G. Meng, F. Chen, Improving the positional adaptability: structure-based design of biphenyl-substituted diaryltriazines as novel non-nucleoside HIV-1 reverse transcriptase inhibitors, *Acta Pharm. Sin. B* 10 (2020) 344–357.
- [30] Z. Huo, H. Zhang, D. Kang, Z. Zhou, G. Wu, S. Desta, X. Zuo, Z. Wang, L. Jing, X. Ding, D. Daelemans, E. De Clercq, C. Pannecouque, P. Zhan, X. Liu, Discovery of novel diarylpyrimidine derivatives as potent HIV-1 NNRTIs targeting the “NNRTI Adjacent” binding site, *ACS Med. Chem. Lett.* 9 (2018) 334–338.
- [31] B. Huang, W. Chen, T. Zhao, Z. Li, X. Jiang, T. Ginex, D. Vilchez, F.J. Luque, D. Kang, P. Gao, J. Zhang, Y. Tian, D. Daelemans, E. De Clercq, C. Pannecouque, P. Zhan, X. Liu, Exploiting the tolerant region I of the non-nucleoside reverse transcriptase inhibitor (NNRTI) binding pocket: discovery of potent diarylpyrimidine-typed HIV-1 NNRTIs against wild-type and E138K mutant virus with significantly improved water solubility and favorable safety profiles, *J. Med. Chem.* 62 (2019) 2083–2098.
- [32] S. Castellino, M.R. Groseclose, J. Sigafos, D. Wagner, M. de Serres, J.W. Polli, E. Romach, J. Myer, B. Hamilton, Central nervous system disposition and metabolism of Fosdevirine (GSK2248761), a non-nucleoside reverse transcriptase inhibitor: an LC-MS and Matrix-assisted laser desorption/ionization imaging MS investigation into central nervous system toxicity, *Chem. Res. Toxicol.* 26 (2013) 241–251.
- [33] A. Basiri, B.M. Abd Razik, M.O. Ezzat, Y. Kia, R.S. Kumar, A.I. Almansour, N. Arumugam, V. Murugaiyah, Synthesis and cholinesterase inhibitory activity study of new piperidone grafted spiropyrrolidines, *Bioorg. Chem.* 75 (2017) 210–216.
- [34] Z. Wang, D. Kang, M. Chen, G. Wu, D. Feng, T. Zhao, Z. Zhou, Z. Huo, L. Jing, X. Zuo, D. Daelemans, E. De Clercq, C. Pannecouque, P. Zhan, X. Liu, Design, synthesis, and antiviral evaluation of novel hydrazone-substituted thiophene

- [35] [3,2-d]pyrimidine derivatives as potent human immunodeficiency virus-1 inhibitors, *Chem. Biol. Drug Des.* 92 (2018) 2009–2021.
- [36] D. Kang, H. Zhang, Z. Wang, T. Zhao, T. Ginex, F.J. Luque, Y. Yang, G. Wu, D. Feng, F. Wei, J. Zhang, E. De Clercq, C. Pannecouque, C.H. Chen, K.H. Lee, N.A. Murugan, T.A. Steitz, P. Zhan, X. Liu, Identification of dihydrofuro[3,4-d]pyrimidine derivatives as novel HIV-1 non-nucleoside reverse transcriptase inhibitors with promising antiviral activities and desirable physicochemical properties, *J. Med. Chem.* 62 (2019) 1484–1501.
- [37] D.E. Clark, S.D. Pickett, Computational methods for the prediction of 'drug-likeness', *Drug Discov. Today* 5 (2000) 49–58.
- [38] K. Palm, P. Stenberg, K. Luthman, P. Artursson, Polar molecular surface properties predict the intestinal absorption of drugs in humans, *Pharm. Res.* 14 (1997) 568–571.
- [39] J.P. Havens, A.T. Podany, K.K. Scarsi, C.V. Fletcher, Clinical pharmacokinetics and pharmacodynamics of etravirine: an updated review, *Clin. Pharmacokinet.* 59 (2020) 137–154.
- [40] R. Pauwels, J. Balzarini, M. Baba, R. Snoeck, D. Schols, P. Herdewijn, J. Desmyter, E. De Clercq, Rapid and automated tetrazolium-based colorimetric assay for the detection of anti-HIV compounds, *J. Virol. Methods* 20 (1988) 309–321.
- [41] C. Pannecouque, D. Daelemans, E. De Clercq, Tetrazolium-based colorimetric assay for the detection of HIV replication inhibitors: revisited 20 years later, *Nat. Protoc.* 3 (2008) 427–434.
- [42] K. Suzuki, B.P. Craddock, N. Okamoto, T. Kano, R.T. Steigbigel, Poly A-linked colorimetric microtiter plate assay for HIV reverse transcriptase, *J. Virol. Methods* 44 (1993) 189–198.
- [43] Z. Zhou, T. Liu, G. Wu, D. Kang, Z. Fu, Z. Wang, E. De Clercq, C. Pannecouque, P. Zhan, X. Liu, Targeting the hydrophobic channel of NNIBP: discovery of novel 1,2,3-triazole-derived diarylpyrimidines as novel HIV-1 NNRTIs with high potency against wild-type and K103N mutant virus, *Org. Biomol. Chem.* 17 (2019) 3202–3217.